Remote Sensing of Environment 248 (2020) 111969

Contents lists available at ScienceDirect

Remote Sensing of Environment

journal homepage: www.elsevier.com/locate/rse

Short-term vegetation loss versus decadal degradation of grasslands in the Caucasus based on Cumulative Endmember Fractions

Katarzyna Ewa Lewińska[a,*], Patrick Hostert[b,c], Johanna Buchner[a], Benjamin Bleyhl[b], Volker C. Radeloff[a]

[a] SILVIS Lab, Department of Forest and Wildlife Ecology, University of Wisconsin-Madison, 1630 Linden Drive, Madison, WI 53706, USA
[b] Geography Department, Humboldt-Universität zu Berlin, Unter den Linden 6, 10099 Berlin, Germany
[c] Integrative Research Institute on Transformations of Human-Environment Systems (IRI THESys), Humboldt-Universität zu Berlin, Unter den Linden 6, 10099 Berlin, Germany

ARTICLE INFO

Keywords:
Land degradation
Rangelands
Spectral mixture analysis (SMA)
MODIS
Caucasus mountains
LandTrendr
Landsat
Google earth engine

ABSTRACT

Land degradation affects over one-third of the global land area and is projected to become even more widespread due to climate change and land use pressures. Despite being a critical issue for climate change mitigation, biodiversity conservation, and food security, the detection of the onset, duration, and magnitude of land degradation remains challenging, as is early identification of short-term vegetation loss preceding land degradation. Here, we present a new approach for monitoring both short-term vegetation loss and decadal degradation in grasslands using satellite data. Our approach integrates Spectral Mixture Analysis and temporal segmentation, and analyzes dense time-series of satellite observations in three steps. First, we unmix all available satellite observations and aggregate them into monthly composites. Second, we calculate the annual Cumulative Endmember Fractions and examine their piecewise trends among years to determine the onset, duration, and magnitude of short-term vegetation loss and decadal degradation. Third, we attribute a decrease in the green vegetation fraction with a concomitant increase in either open soil, or non-photosynthetic vegetation. We tested our method mapping short-term vegetation loss and decadal degradation in grasslands in the Caucasus Ecoregion using the 2001–2018 time series of MODIS 8-day reflectance data. We found strong patterns of short-term vegetation loss and decadal degradation, mostly in the eastern part of the Caucasus Ecoregion in areas of desert- and semi-desert natural vegetation. Short-term vegetation loss episodes (3–9 years) were more common and had greater magnitude than decadal degradation (≥10 years), especially in steppe regions. On average, 9.3% of grassland area was subjected annually to either decadal, or short-term vegetation loss. Desiccation, i.e., the shift from green vegetation to dry vegetation, was the most prevalent type of change pathway, with green vegetation loss to open soil coming second. Decadal degradation and short-term vegetation loss rates were the highest in dry areas where the potential natural vegetation is sub-shrub deserts, or halophytic, alluvial, and wet lowland forests. Our findings support known general degradation patterns in the Caucasus Ecoregion, but provide better understanding of ongoing processes, by detecting exact location, timing, and magnitude of changes. More broadly, our method advances the monitoring of grasslands by detecting both decadal degradation and short-term vegetation loss. This flexibility supports adaptive degradation monitoring, aids sustainable land management, and provides new information for carbon stock analyses and biodiversity conservation.

1. Introduction

Degradation is one of the most pressing, yet challenging, global environmental problems (IPCC, 2019; UNCCD, 2017a). Caused by both climate change and land use intensification (Cowie et al., 2011), land degradation negatively affects the environment, economy, and public life (Aronson and Alexander, 2013; FAO, 2011; Hassan et al., 2005; IPCC, 2019). Despite general awareness of widespread land degradation (Hassan et al., 2005; IPCC, 2019; UN General Assembly, 2010; UNCCD, 2017a), statistics on the extent, duration, and severity of degradation vary widely (Gibbs and Salmon, 2015). This is partly due to the plethora of different types of degradation, combined with a variety of land degradation definitions, and numerous detection methods (Jamsranjav et al., 2018; Reed et al., 2011; Vogt et al., 2011; Yengoh et al., 2015).

* Corresponding author.
E-mail address: lewinska@wisc.edu (K.E. Lewińska).

https://doi.org/10.1016/j.rse.2020.111969
Received 27 January 2020; Received in revised form 17 May 2020; Accepted 27 June 2020

Consequently, land degradation is often acknowledged but rarely accounted for in analyses of climate change, carbon pools, biodiversity, and food security (Balkovič et al., 2018; Barbut and Alexander, 2015; Mitchard, 2018).

Land degradation is a global phenomenon, but its effects are the most severe in arid, semi-arid and sub-humid regions (Cowie et al., 2011; Gisladottir and Stocking, 2005). Grassland ecosystems in drylands, i.e., rangelands, are especially prone to degradation when biotic degradation factors (e.g., lack of precipitation) are coupled with abiotic degradation factors (e.g., exploitative land management, such as overgrazing; Cherlet et al., 2018; IPCC, 2019; De Leeuw et al., 2019). Alpine meadows, and temperate grasslands also experience degradation (Gao et al., 2010; Wen et al., 2013). Although grassland degradation outside of dry regions is less studied and not recognized by the United Nations Convention to Combat Desertification (UNCCD), it has become a one of the monitoring priorities within the framework of Land Degradation Neutrality (Cowie et al., 2018; UNCCD, 2017b).

Many land degradation definitions and mapping techniques focus on changes in aboveground vegetation condition (e.g.,Q. Gao et al. 2006; Kuemmerle et al., 2006; Zhang et al., 2016). This simplification neglects other important aspects of degradation, such as loss of species diversity, altered plant species composition, soil erosion, or lower nutritional value of plants (Andrade et al., 2015; Dlamini et al., 2014; Mansour et al., 2016; Neudert et al., 2013). However, assessing land degradation based on changes in aboveground vegetation condition and productivity provides a straightforward approximation of land functions and capacities, and allows the use of remote sensing (Dubovyk, 2017).

Remote sensing data and techniques can effectively map and monitor land degradation in many biomes and regions (Bai et al., 2008; Gibbs and Salmon, 2015; Main-Knorn et al., 2013; Zhou et al., 2017), including drylands (Fensholt et al., 2013; Horion et al., 2014; Hostert et al., 2003). Long time series of satellite observations are especially useful (Bai et al., 2008; Song et al., 2018; Tindall et al., 2012), and frequent intra-annual observations allow to distinguish degradation from variability in inter-annual phenology (Horion et al., 2014; Verbesselt et al., 2010a, 2010b). Because of the frequent observations, MODIS data are particularly valuable for land degradation detection (Dubovyk et al., 2013; Eckert et al., 2015).

Vegetation indices, such as NDVI, have been extensively used in land degradation studies (de Jong et al., 2011; Fensholt and Proud, 2012), but physically-based approaches, such as Spectral Mixture Analysis (SMA; Adams and Smith (1986)) have two distinct advantages. First, SMA utilizes information from all spectral bands of a given satellite sensor, which improves estimates of the fraction of ground cover of each target component (endmember), such as green vegetation, soil, or non-photosynthetic vegetation. This is especially important where vegetation is sparse and soil reflectance affects vegetation indices (Elmore et al., 2000; Huete et al., 1985; Smith et al., 2019). Second, since SMA is based on physically-meaningful endmembers, interpretation of results is straightforward and directly linked to the underlying processes. Although early degradation studies in semi-arid regions found marginal differences between maximum greenness vegetation indices and SMA results (Sonnenschein et al., 2011), within-year time series of endmember fractions can enhance degradation detection (Suess et al., 2018; Tindall et al., 2012), and identify even subtle intra-annual changes (Bullock et al., 2019; Schultz et al., 2016).

Land degradation is typically defined as long-term loss of productivity and ecosystem functions, and hence is usually monitored using long-term trend analyses (Bai et al., 2008; Song et al., 2018). However, some degradation processes occur rapidly (e.g., water erosion), or are characterized by pulses of change (e.g., recurring dry spells, selective logging in tropical forest) (Bullock et al., 2018; de Jong et al., 2012). Such short-term changes are easily overlooked in long-term degradation analyses, even when they are of considerable magnitude (Wessels et al., 2012). Trajectory-based change detection algorithms, such as LandTrendr (Kennedy et al., 2010), BFAST (Verbesselt et al., 2012; Verbesselt et al., 2010a; Verbesselt et al., 2010b) or vegetation change tracker (VCT; Huang et al. (2010)), allow to identify both short-term vegetation loss and decadal degradation. The ability to detect short-term vegetation loss is particularly important for sustainable land management and allows to better understand degradation development and dynamism, providing an early warning. Furthermore, monitoring short-term vegetation loss due to both natural, as well as anthropogenic causes supports carbon emission monitoring and allows an interim evaluation of progress towards Land Degradation Neutrality goals (Cowie et al., 2018; UNCCD, 2017b).

Our overarching goal was to develop a new remote sensing-based approach to monitor both short-term vegetation loss (< 10 years) and decadal degradation (≥ 10 years) in grasslands. We designed our method to: i) be applicable to any grassland ecosystem; ii) detect both short-term vegetation loss and decadal degradation episodes, and estimate their location, timing and magnitude; and iii) quantify different types of change, i.e., shifts among fractions of ground cover. To do so, we combined dense (minimum monthly) satellite time series, SMA, and pixel-based detection of temporal trajectories realized with LandTrendr (Kennedy et al., 2010). We demonstrated the capability of our approach mapping short-term vegetation loss and decadal degradation in grasslands in the Caucasus Ecoregion. Specifically, our objectives were to: i) identify location, frequency and magnitude of short-term vegetation loss and decadal degradation episodes; ii) compare short-term vegetation loss and decadal degradation within different natural vegetation formations.

2. Methods

2.1. Study area

We tested our approach in the diverse grassland ecosystems of the Caucasus Ecoregion. The Caucasus Ecoregion (580,000 km^2) is centered around the Caucasus Mountains between the Black Sea and the Caspian Sea (Fig. 1). The complex topography results in a wide range of climatic conditions, with the NW-SE precipitation gradient ranging from 4100 to 300 mm (or below) (Volodicheva, 2002). Consequently, the Caucasus region is characterized by a high number of landscapes (*Caucasus Environment* Outlook, 2002; Zazanashvili et al., 2000) and is a global hotspot of biodiversity (Marchese, 2015; Tishkov and Belonovskaya, 2012). Vegetation types range from nival to forests to desert vegetation (Bohn et al., 2007; Bohn et al., 2004).

Geographical diversity and a long history of land use have resulted in a great variety of grassland ecosystems present in the region (Belonovskaya et al., 2016; Lachashvili et al., 2017; Zazanashvili et al., 2000). Animal husbandry is an important part of the local economy and identity (Neudert and Allahverdiyeva, 2009). High grazing pressure (De Leeuw et al., 2019; Shatberashvili et al., 2015) combined with unfavorable climate changes (Elizbarashvili et al., 2017; Shatberashvili et al., 2015; Zoï Environment Network, 2011) are a threat for grasslands in the region, and can cause degradation (NACRES, 2013; Neudert et al., 2013; Tepanosyan et al., 2017).

2.2. Satellite data

We analyzed the 2001–2018 time series of the 8-day 500 m MODIS surface spectral reflectance product (MOD09A1; Collection 6) available in Google Earth Engine (GEE; (Gorelick et al., 2017); data accessed in May 2019). The Collection 6 MOD09A1 product is atmospherically corrected (Vermote et al., 2002) and adjusted for sensor degradation (Lyapustin et al., 2014). We screened each scene using the inherent 'StateQA' (Quality Assessment) band, and excluded all pixels with low quality, cloud or snow contamination (bits 0–1, 2–3 and 12, respectively).

To identify region-specific endmembers, we analyzed five Landsat 7

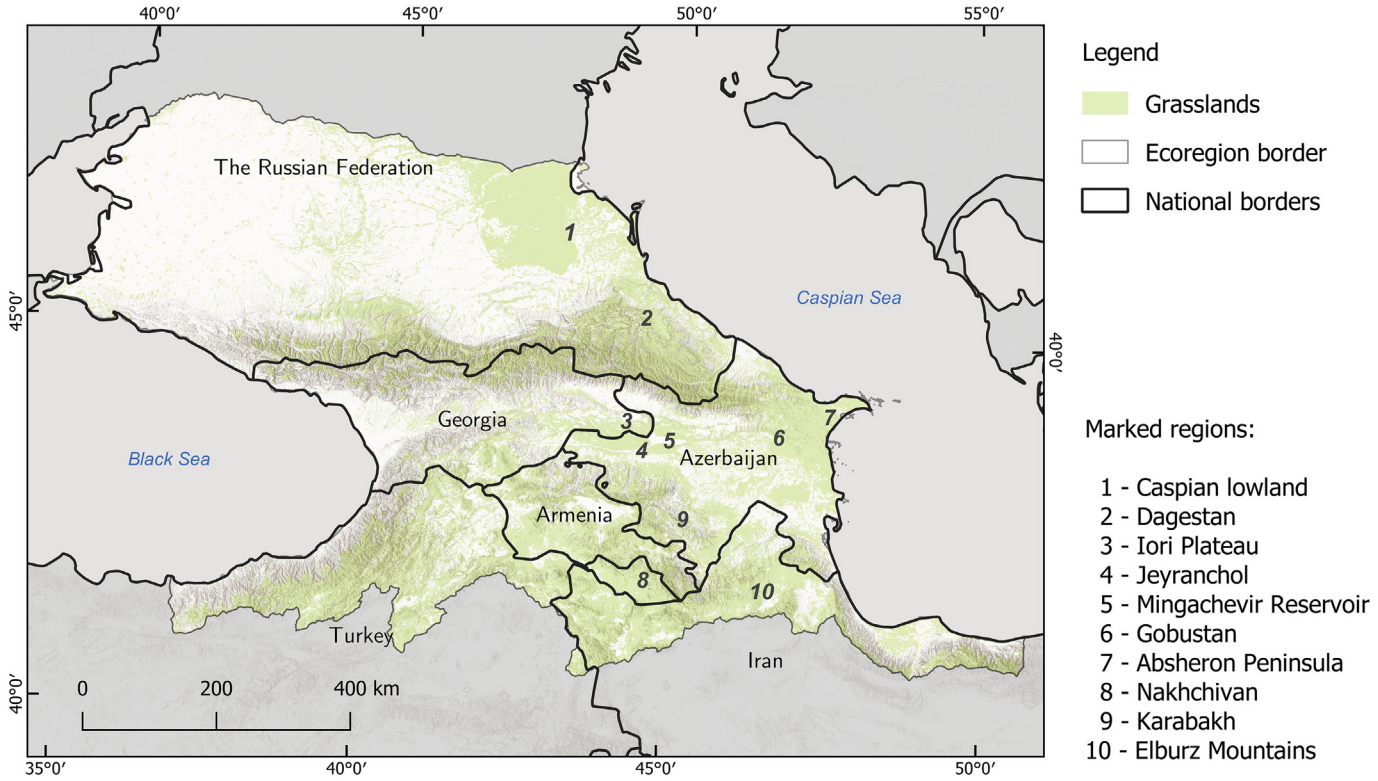

Fig. 1. Location and shade relief of the Caucasus Ecoregion, with regions marked that are discussed in the text.

Enhanced Thematic Mapper plus (ETM+) scenes acquired for footprint 169–031 WRS-2 on 2015-01-04, 2015-04-26, 2015-07-31, 2015-08-16 and 2015-11-20. We selected this footprint because it covers a wide elevational gradient (from 17 to 4481 m a.s.l.), a variety of grassland types including summer and winter pastures, and known degradation hotspots in West Azerbaijan and East Georgia (NACRES, 2013). We chose 2015 as the target year, due to dry weather conditions, which maximized our chances to identify pure soil spectra in the imagery. All Landsat scenes were downloaded from the U.S. Geological Survey (USGS) service as collection 1 tier 1 surface reflectance products. We used the QA bands to remove all pixels flagged as cloud, shadow or snow (Zhu and Woodcock, 2012).

2.3. Ancillary data

We focused on grasslands, i.e., areas classified as 'rangelands', 'sparse vegetation' or 'barren' in the 2015 land cover classifications of Buchner et al. (2020) and Bleyhl et al. (2017), and resampled the 30-m classifications to 500-m MODIS pixels based on majority rule. Furthermore, we used the Map of the Natural Vegetation of Europe (Bohn et al., 2007) to stratify our results. We selected the subgroup level of the classification and included 13 out of 24 formations present in the Caucasus Ecoregion, dismissing classes smaller than 7000 km^2. The dataset covers Armenia, Azerbaijan, Georgia and the Russian Caucasus (Fig. S1).

2.4. Cumulative endmember fractions: Concept

Conceptually, a pixel in a grassland area can comprise up to three types of ground cover: soil (or rock), green vegetation, and non-photosynthetic vegetation, plus shade (Sonnenschein et al., 2011; Suess et al., 2018). While the ground cover types reflect vegetation density and composition, the shade accounts for micro-shadowing at the subpixel level and illumination effects at the regional level (Elmore et al., 2000; Kuemmerle et al., 2006). SMA aims at quantifying the share of different components within a pixel based on their respective endmembers, assuming linear combination of the spectra:

$$\rho_j = \sum_{i=0}^{n} f_i * \rho_{i,j} + e_j \quad (1)$$

where ρ_j is the reflectance in band j, f_i is a fraction of endmember i, $\rho_{i,j}$ is a spectrum of endmember i in band j, and e_j is an residual term for band j. We assumed that there were no other ground cover types, and applied a constrained non-negative SMA model, which limited endmember fractions to positive values, and enforced they summed to 1.

The acquisition date of the analyzed satellite image can affect analyses greatly (Sonnenschein et al., 2011), because SMA fractions change over the course of a year due to phenology (Kuemmerle et al., 2006; Somers et al., 2011) and illumination effects (Elmore et al., 2000). Alternatively, the effects of phenology and illumination conditions in a dense time series (e.g., monthly observations) can be 'normalized' by summing endmember fractions over a period of one year, akin to common practice in vegetation productivity studies (e.g., Hobi et al., 2017; Reed et al., 1994). The resulting annual sum captures the full range of illumination conditions and phenology phases, reflecting the vegetation growth for the entire season. This is why we calculate Cumulative Endmember Fractions in order to facilitate a straightforward year-to-year comparison of land cover conditions (Fig. 2). The inherent range of Cumulative Endmember Fractions is from 0 to 1*n, where n is the number of datasets used for unmixing fractions within one year. For better interpretability, we rescaled the Cumulative Endmember Fraction values from 0 to 1.

The relative changes between the shade and non-photosynthetic vegetation fractions are particularly interesting for shrublands (Suess et al., 2018) and can be indicative of shrub encroachment (Kuemmerle et al., 2006). However, the shade fraction is typically less important in grassland ecosystems, where it varies cyclically with phenology (vegetation micro-shadowing) and illumination conditions (topographic shading). Conversion to shrubland is not common in the region, and our grassland mask (see section 2.3.) included only herbaceous vegetation.

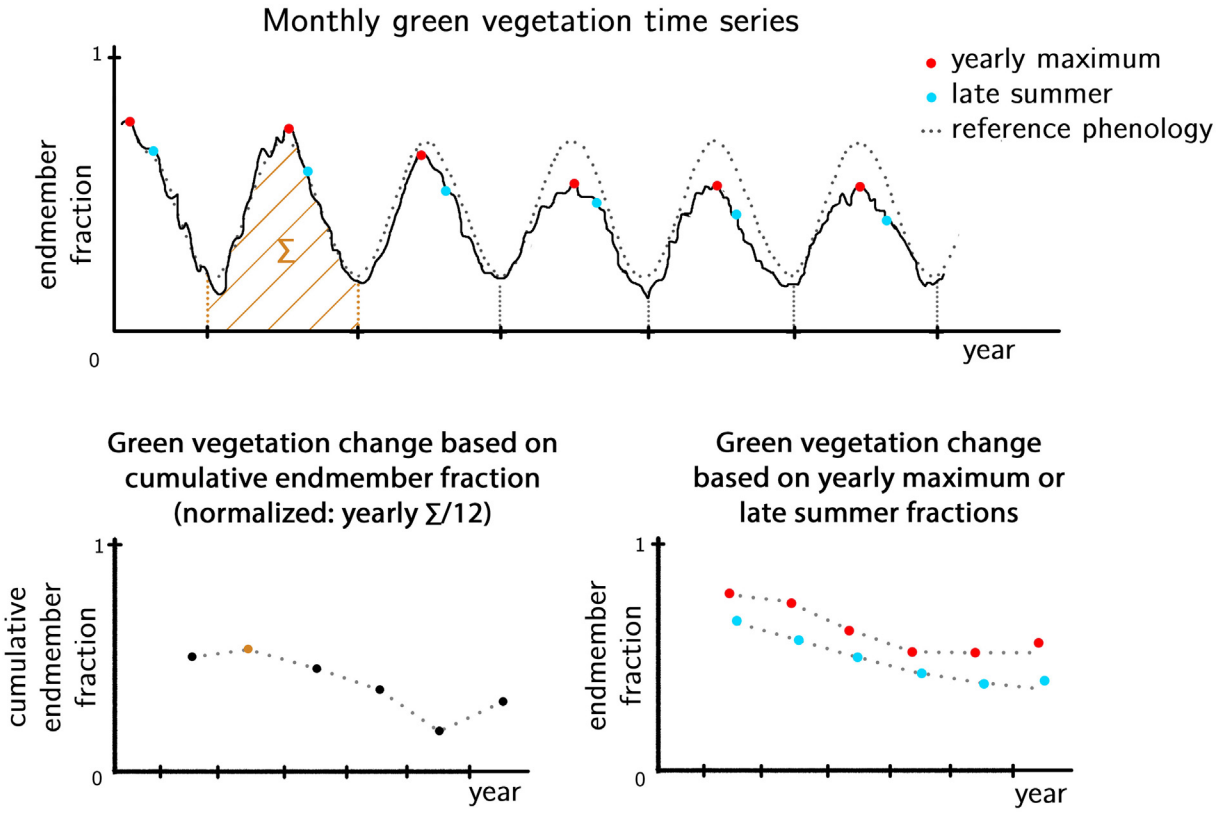

Fig. 2. Cumulative Endmember Fraction values versus yearly maximum and late-summer fractions. The different trajectories in the two bottom graphs highlight the limitations of basing analyses on only one observation per year.

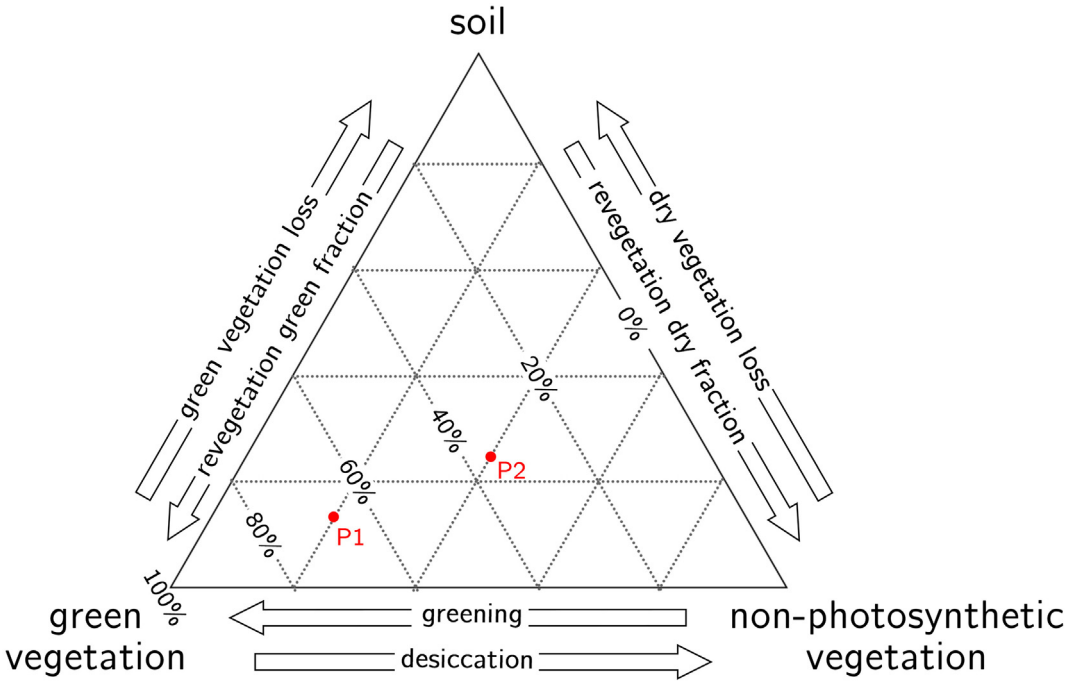

Fig. 3. Grassland land cover composition approximated by soil, green vegetation and non-photosynthetic vegetation fractions. Example points: P1 (soil: 13%, gv: 67%, npv 20%), and P2 (soil: 24%, gv: 36%, npv 40%). Change pathways are labeled on the sides of the graph. For example, the change from P1 to P2 (ΔP soil: 11%, gv: −31%, npv: 20%) means a combination of green vegetation loss and desiccation, with the latter being the dominant change pathway. (For interpretation of the references to colour in this figure legend, the reader is referred to the web version of this article.)

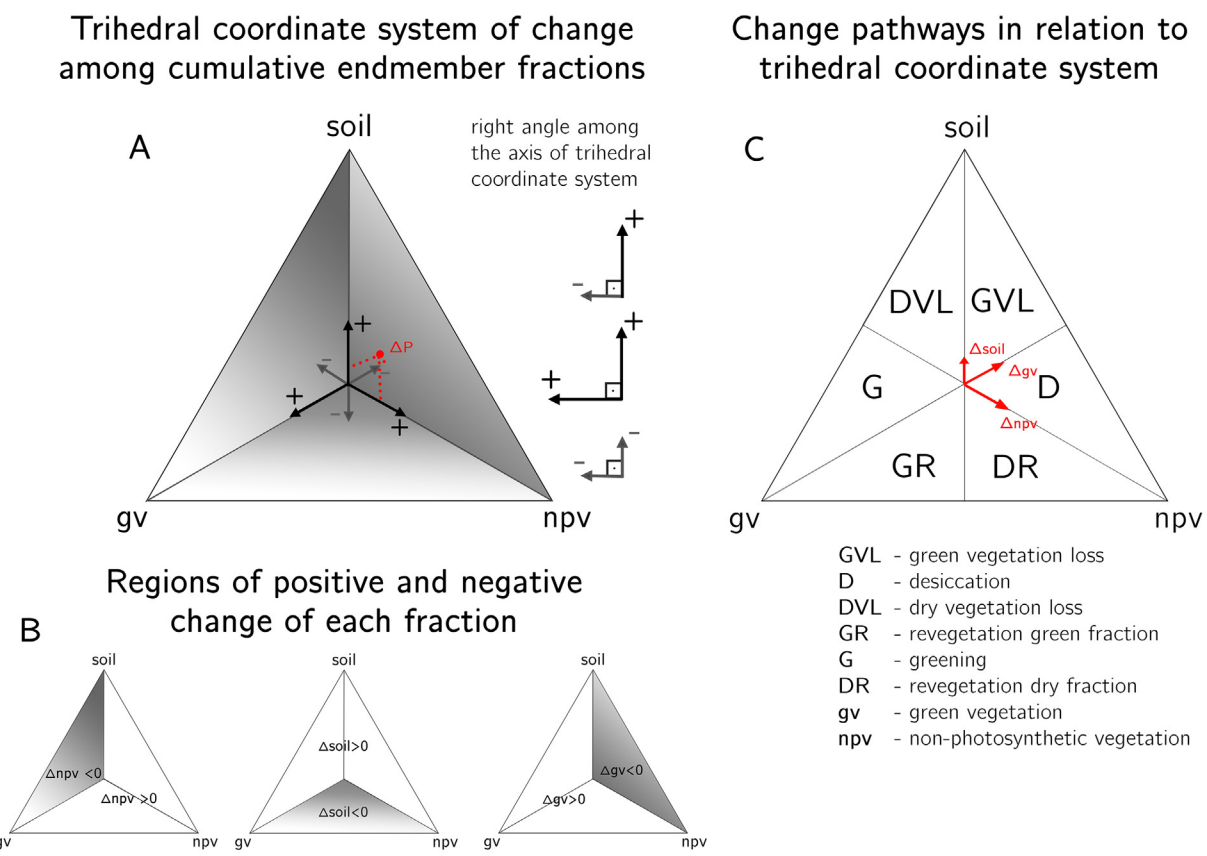

Fig. 4. Trihedral feature-space of a Δ vector quantifying changes in Cumulative Endmembers Fractions between two time steps. A: A trihedral coordinate system of the Δ vector, with the origin of the coordinate system in the common point in the center, the positive half-axes going outwards along the corners between faces, and the negative half-axes being bisectors of trihedral faces' corner angles and normal to the respective positive half-axes. B: location of positive and negative change areas of each fraction. C: Diagram introducing zones in the Δ feature-space associated with each change pathway. ΔP represents the change from P1 to P2 in Fig. 3.

Consequently, we simplified the model and summed the non-photosynthetic vegetation and shade Cumulative Endmember Fractions into one cumulative fraction (hereafter 'non-photosynthetic vegetation'). The resulting three-dimensional Cumulative Endmember Fractions space approximates any grassland area in terms of its soil, green vegetation and non-photosynthetic vegetation fractions (Fig. 3).

Changes in Cumulative Endmember Fractions over time capture different types of vegetation loss or vegetation recovery (e.g., Song et al., 2018; Tindall et al., 2012) and we refer to these as pathways hereafter. Shifts among the endmember fractions are symptomatic, not process-based, e.g., we labeled a shift from green vegetation to soil as green vegetation loss, not overgrazing or erosion (Fig. 3). In grassland ecosystems, green vegetation loss, desiccation and dry vegetation loss are different pathways of negative changes in vegetation cover, whereas revegetation green fraction, greening, and revegetation dry fraction represent positive changes in vegetation cover and condition.

A change in Cumulative Endmember Fractions between two time steps (t1 and t2) can be quantified by a change vector $\Delta = [\Delta soil, \Delta gv, \Delta npv]$, where $\Delta soil = soil_{t2} - soil_{t1}$, $\Delta gv = gv_{t2} - gv_{t1}$ and $\Delta npv = npv_{t2} - npv_{t1}$. Since we use the constrained non-negative SMA model, this means $\Delta soil + \Delta gv + \Delta npv = 0$. The Δ vector can be shown in a trihedral coordinate system (Fig. 4A and B). The origin of the coordinate system is the common point in the center, the positive half-axes go outwards along the corners between faces, and the negative half-axes are bisectors of trihedral faces' corner angles and normal to the respective positive half-axes (Fig. 4A). Each change has interrelated trajectories, i.e., a decrease in green vegetation Cumulative Endmember Fractions leads to an increase in soil and non-photosynthetic vegetation fractions, with one of the pathways dominating over the other. The direction and length of the Δ vector indicate the dominant change pathway and its magnitude, respectively (Fig. 4C).

2.5. Endmember selection

For our SMA, we estimated four endmember fractions: soil, green vegetation, non-photosynthetic vegetation and shade (Sonnenschein et al., 2011; Suess et al., 2018). Lacking reference spectra from the Caucasus, we used image endmembers. The 500-m resolution of the MODIS data makes it difficult to identify spectrally pure pixels, which is why we used Landsat ETM+ data instead (Gao et al., 2006; Hilker et al., 2009; Zhu et al., 2010). Based on eigenvector values from the Minimum Noise Fraction results for five ETM+ datasets we used only the first five Minimum Noise Fraction bands to calculate the Pixel Purity Index for each selected Landsat scene. We visually inspected spectra of all spectrally pure pixels, and identified green vegetation and soil candidate endmembers, making sure all selected endmembers were located at the boundary of the pixel cloud (Sonnenschein et al., 2011). Since the Pixel Purity Index did not identify any non-photosynthetic vegetation spectrum, we selected this endmember from the Ecological Spectral Information System (ECOsis) Spectral Library (https://ecosis.org; accessed on 5th May 2019) and chose spectra from the Daughtry and Hunt (2008).

We identified the final set of endmembers from the pool of candidate endmembers (soil, green vegetation and non-photosynthetic vegetation), ensuring the lowest correlation between the final set of spectra (Meer and Jia, 2012). Finally, we added the shade endmember (Fig. 5, Table S1) (Bullock et al., 2018; Smith et al., 1990; Sonnenschein et al., 2011). We defined the shade endmember as 0.0001, i.e., a spectrum with reflectance close to zero (an application of the traditionally used 0 reflectance definition of shade was impossible due to

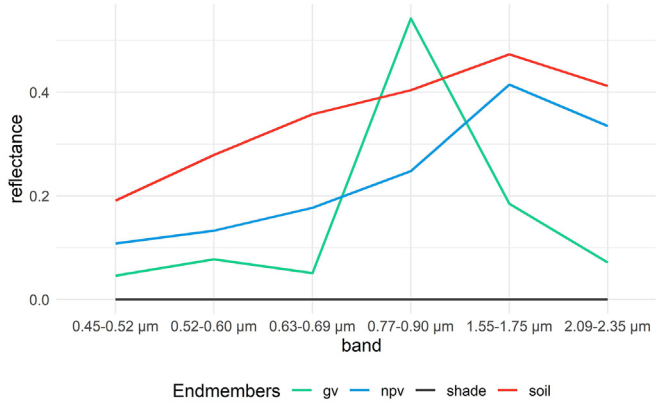

Fig. 5. Reflectance of soil, green vegetation (gv), non-photosynthetic vegetation (npv) and shade endmembers for the Landsat ETM + bands. Spectra values in Table S1. (For interpretation of the references to colour in this figure legend, the reader is referred to the web version of this article.)

computational limitations of GEE's unmixing function). We evaluated the performance of the identified endmembers during a field visit in early July 2019 (Supplement S1).

2.6. Endmembers time series

We ran the SMA for every MOD09A1 scene available for our study site in Google Earth Engine as of May 2019. We excluded MODIS band 5, because there is no equivalent TM/ETM + band. We aggregated the resulting time series to monthly observations (Fig. 6). When multiple observations were available for a pixel in a given month, we selected the set of endmember fractions with the highest green vegetation value. We calculated the Cumulative Endmember Fractions for each year from 2001 to 2018 based on the monthly endmember fraction values (Fig. 6; compare section 2.4). Pixels with missing observations for a given year were masked out for that year only. Grasslands at high elevations, such as summer pastures and alpine meadows, were largely omitted due to snow cover in winter months (an area of approximately 40,970 km^2).

2.7. LandTrendr analysis and vegetation loss in grasslands

In order to estimate the onset, duration, and magnitude of both short-term vegetation loss and decadal degradation episodes, we ran LandTrendr in GEE on the 2001–2018 time series of the green vegetation Cumulative Endmember Fraction. LandTrendr identifies for each pixel piecewise linear trend segments in spectral time series (Kennedy et al., 2018; Kennedy et al., 2010). The trends are fitted based on a selection of user defined criteria including the minimum number of observations in the time series, maximum number of allowed segments to be fitted to the time series, criteria for outlier detection, minimum recovery period after detected disturbance, and the *p*-value of the overall model fit. We used default LandTrendr control parameters (Kennedy et al., 2018, Kennedy et al., 2010), and allowed a maximum of 8 segments, a one-year recovery period, and a minimum of 15 observations in the time series. We also decided to preserve all spikes in the time series, assuming that data preprocessing and aggregation eliminated erroneous values.

We analyzed the magnitude of each vegetation loss episode in the LandTrendr results based on the real values, not the values fitted by LandTrendr. We thereby preserved the constraints of the SMA model inherited by the Cumulative Endmember Fractions, which are essential to recognize change pathways calculated as shifts among fractions (Section 2.4). We calculated magnitude of each trend segment as the absolute change in green vegetation Cumulative Endmember Fraction between its first and the last year. Since the LandTrendr algorithm identifies a trend segment on a vertex-to-vertex basis, the first year of each identified segment represents a 'pre change' state. To account for this, we reported the timing of our vegetation loss results starting from the second year of each trend segment, which corresponds to the first year we observed decline in green vegetation Cumulative Endmember Fraction.

We defined a vegetation loss episode as being at least three years long and having a magnitude of at least 10% of the per-pixel maximum green vegetation Cumulative Endmember Fraction in the entire time series. We classified the vegetation loss episodes identified by LandTrendr into two classes: i) short-term vegetation loss episodes lasting from 3 to 9 years, and ii) decadal degradation episodes lasting 10 years or more. For each vegetation loss episode, we recorded its

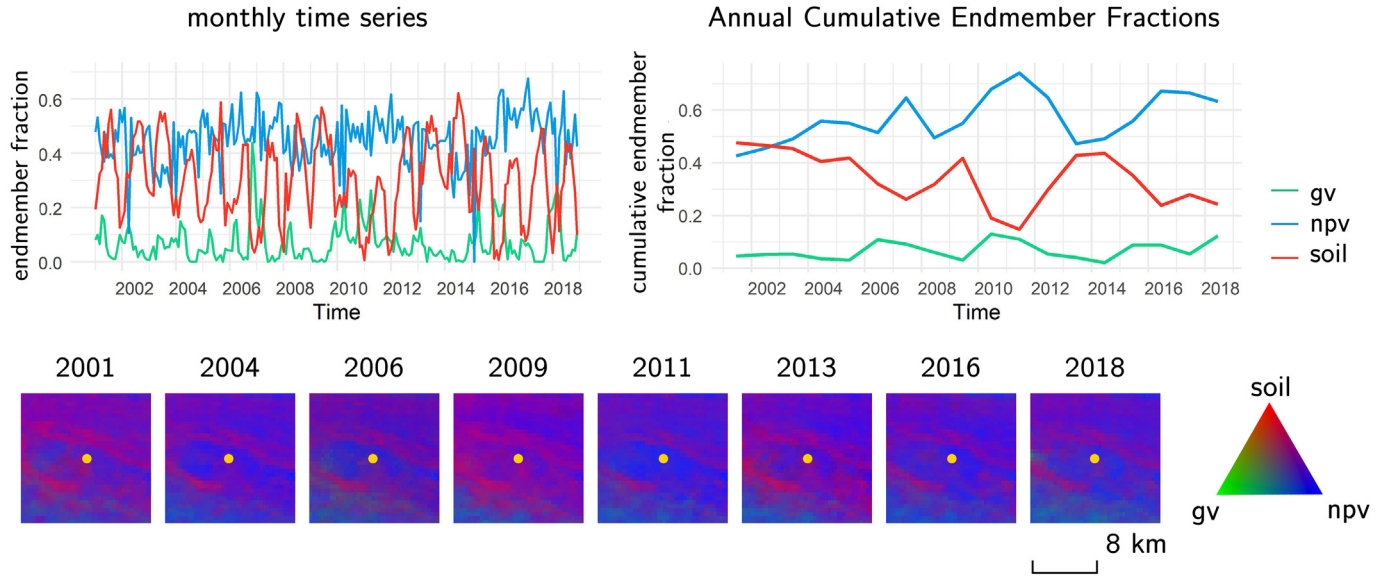

Fig. 6. Monthly soil, green vegetation (gv) and non-photosynthetic vegetation (npv) fraction time series, as well as the corresponding Cumulative Endmember Fractions. The bottom row shows selected soil-gv-npv composites of the annual Cumulative Endmember Fractions for the area surrounding the pixel (yellow dot) for which temporal variability is shown above. Endmember fraction and Cumulative Endmember Fraction are scaled between 0 and 1. (For interpretation of the references to colour in this figure legend, the reader is referred to the web version of this article.)

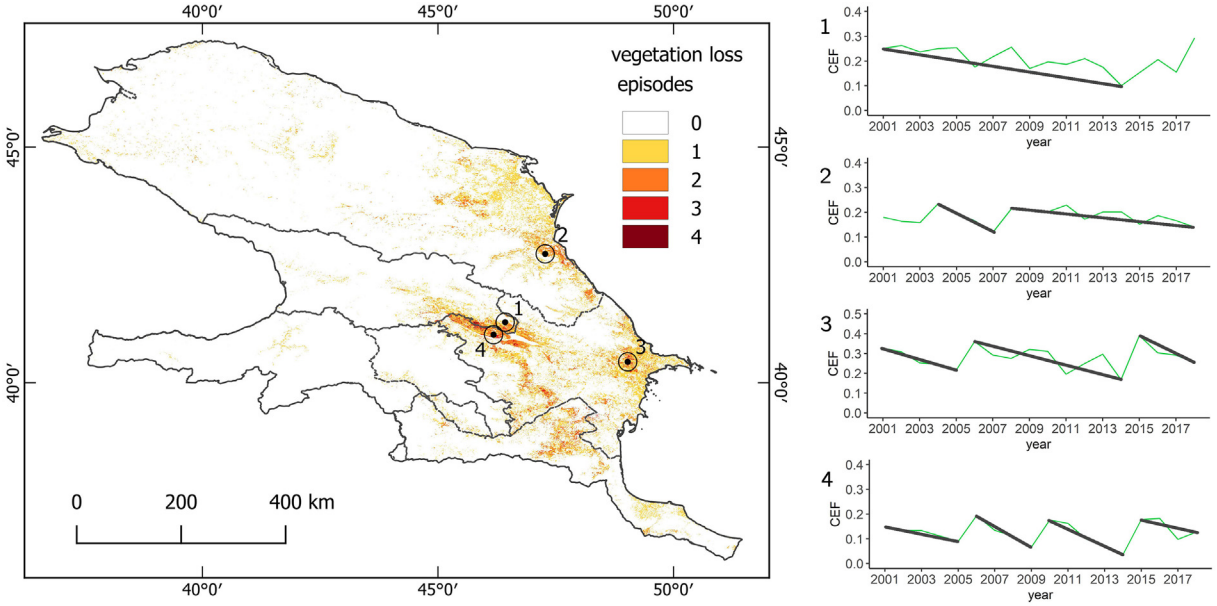

Fig. 7. Number of vegetation loss episodes (short-term vegetation loss and decadal degradation together) between 2001 and 2018. The right panel shows examples of linear trend segments corresponding to short-term vegetation loss and decadal degradation changes in the green vegetation Cumulative Endmember Fraction (CEF). (For interpretation of the references to colour in this figure legend, the reader is referred to the web version of this article.)

magnitude and identified the dominant change pathway. We used ANOVA to test for significance in the differences in green vegetation loss magnitude of short-term vegetation loss and decadal degradation episodes. Finally we compared the dominant vegetation loss change pathways for different Natural Vegetation formations (Bohn et al., 2007). We reported areas with a precision of 25 km^2, which corresponds to 0.5% of the total area of the Natural Vegetation formations. This accounted for the uncertainty in the SMA and LandTrendr analyses.

3. Results

3.1. Short-term vegetation loss and decadal degradation in grasslands in the Caucasus ecoregion

We found that approximately 49,825 km^2 of grasslands (16.9% of all grasslands and 8.5% of the ecoregion) experienced at least one vegetation loss episode (short-term vegetation loss or decadal degradation) between 2001 and 2018 (Fig. 7). Most of the vegetation loss occurred in the eastern Caucasus, with hotspots in the Caspian lowland, Gobustan, Elburz Mountains, and around the Mingachevir Reservoir. The majority of areas (approximately 37,550 km^2) experienced only a single vegetation loss episode, but there were also regions with two, three or even four consecutive vegetation loss episodes, which affected approximately 11,075 km^2, 1175 km^2 and 50 km^2, respectively.

On average, 27,400 km^2 (9.3% of all grasslands and 4.7% of the ecoregion area) was subjected to vegetation loss (short-term vegetation loss or decadal degradation) in a given year (Fig. 8). The greatest number of new short-term vegetation loss episodes started in 2011 and 2016. Especially in 2011, many very strong short-term vegetation loss episodes initiated near the Mingachevir Reservoir, Karabakh, and in the Eastern part of Dagestan (Fig. S2).

3.2. Vegetation loss dynamism: Short-term vegetation loss vs. decadal degradation

We found that approximately 14,075 km^2 (4.8% of grasslands and 2.4% of the ecoregion) experienced decadal (≥10 year-long) degradation between 2001 and 2018 (Fig. 9A), the magnitudes of which ranged from −0.01 to −0.31. Major decadal degradation occurred in Gobustan, the Caspian lowland, Karabakh and Dagestan, and most of the episodes started in 2002 (Fig. 9B). In the Caspian lowland region, decadal degradation episodes started mainly between 2002 and 2007, and in NE-Dagestan in 2009.

We mapped four different symptomatic change pathways in the areas that experienced decadal degradation (Fig. 10A). Desiccation was the most prevalent dominant pathway (approximately 9200 km^2, 65.7% of the area of decadal degradation), and was especially frequent in the Caspian Lowlands, Dagestan, Gobustan, the Iori Plateau, and the Elburz mountains. This change pathway had the biggest overall magnitude. Green vegetation loss was the second most common dominant change pathway (approximately 2300 km^2, 16.5%), and occurred mainly along the coastline of the Caspian Lowlands, and in Karabakh, Gobustan and the Absheron Peninsula. We found that approximately 2050 km^2 (14.7%) of all grasslands underwent revegetation dry fraction, especially in the Caspian Lowlands, Gobustan, Jeyranchol and NW- Nakhchivan.

Short-term vegetation loss (< 10 year-long) occurred on approximately 40,075 km^2 (13.6% of grasslands and 6.9% of the ecoregion) and some places experienced multiple short-term vegetation loss episodes (Fig. 11). Five regions were short-term vegetation loss hotspots: the area surrounding the Mingachevir Reservoir, Gobustan, Degradation, the Caspian Lowlands, and Karabakh including the Elburz Mountains. The strongest and most frequent short-term vegetation loss episodes occurred near Mingachevir Reservoir, where we detected up to four episodes starting in 2002, 2007, 2011, and 2016, respectively. In Gobustan moderately strong short-term vegetation loss episodes were initiated mainly in 2002, 2007, and 2016. Degradation in Dagestan started predominantly in 2002, 2007, 2011, and 2015–2016. In the Caspian Lowlands, and in northern Dagestan short-term vegetation loss started as late as 2011–2012, with second episodes initiated in 2016. We observed up to three subsequent short-term vegetation loss episodes starting in 2002, 2010–2011 and 2016 in Karabakh and northern fringes of the Elburz Mountains.

Desiccation was the most common dominant short-term vegetation loss pathway, representing 71.3% of all cases (Fig. 10A and B, Fig. S3), whereas 18.7% reflected the green vegetation loss pathway. Dry vegetation loss occurred only in 2% of the area, but this pathway had the

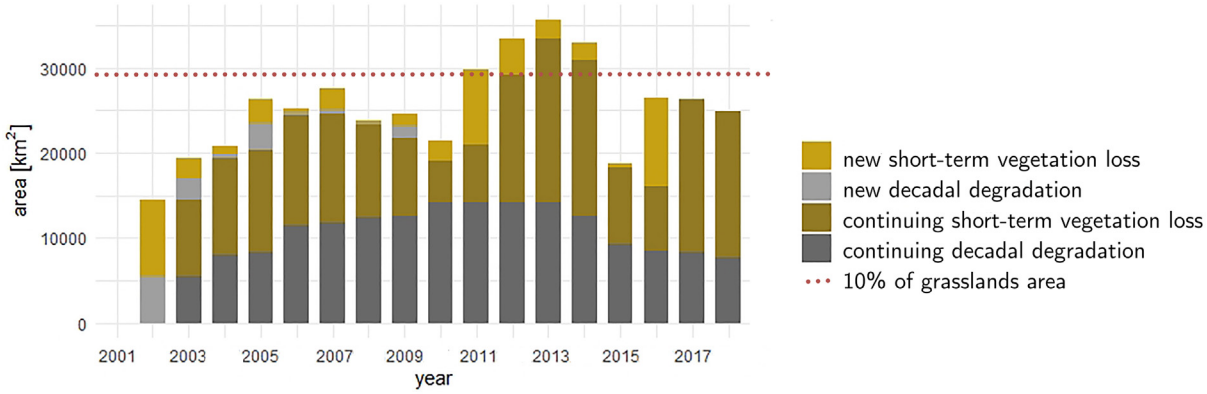

Fig. 8. The total area of continuing and newly initiated short-term vegetation loss and decadal degradation episodes for each year from 2001 through 2018. Since we required a short-term vegetation loss episode to be at least 3 years long, we did not identify any new short-term vegetation loss onset for the last two years of the time series, and no new decadal degradation after 2009. For a map of the continuing degradation for each year see Fig. S2.

greatest change magnitude. The area dominated by revegetation of dry fraction was equivalent to 7.8% of all areas affected by short-term degradation.

3.3. Short-term vegetation loss and decadal degradation within natural vegetation formations

Short-term vegetation loss was most widespread in the rangelands of the Caucasus Ecoregion and particularly common in areas where the potential natural vegetation is sub-shrub deserts, halophytic vegetation, and alluvial and wet lowland forests (Table 1). Within those formations > 40% of the grasslands had at least one vegetation loss episode between 2001 and 2018. Short-term vegetation loss was also very frequent in areas characterized by hygrophilous mixed forests, reed vegetation, Caucasian mixed hornbeam-oak forests, and true steppe. Decadal degradation trends affected > 19% of grasslands in reed and halophytic natural vegetation formations. In alluvial and wet lowland forest and sub-shrub deserts decadal degradation was less common, yet still we detected it in > 9% of grasslands there. Vegetation loss (both, short-term vegetation loss or decadal degradation) in grasslands in alpine, subalpine, and montane to altimontane zones was very low (mostly below 25 km^2).

In all potential natural vegetation types, short-term vegetation loss episodes had greater change magnitude than decadal trends (Fig. 12). The effect of vegetation loss episode length on magnitude of green vegetation loss was strong and highly significant (ANOVA, F = 20,930, $p < .001$). Differences in magnitude of green vegetation loss were also highly significant among vegetation types (F = 716, $p < .001$). Steppe vegetation formations had the greatest difference in green vegetation loss magnitude between short-term vegetation loss and decadal degradation episodes (Fig. 12).

Desiccation was by far the most common change pathway within all natural vegetation formations for both short-term vegetation loss and decadal degradation (Table 2). Grasslands in semiarid and arid climate (L.1, M.1, M.2, O.2, and P.2) had the highest variation in short-term vegetation loss and degradation change pathways. Decadal degradation was typically related to green vegetation loss and revegetation of dry fraction. Within areas of halophytic and sub-shrub deserts potential vegetation, green vegetation loss represented between 24% and 38% of all detected short-term vegetation loss and decadal degradation, respectively. Grasslands in sub-alpine vegetation types had relatively high dry revegetation, especially for decadal degradation.

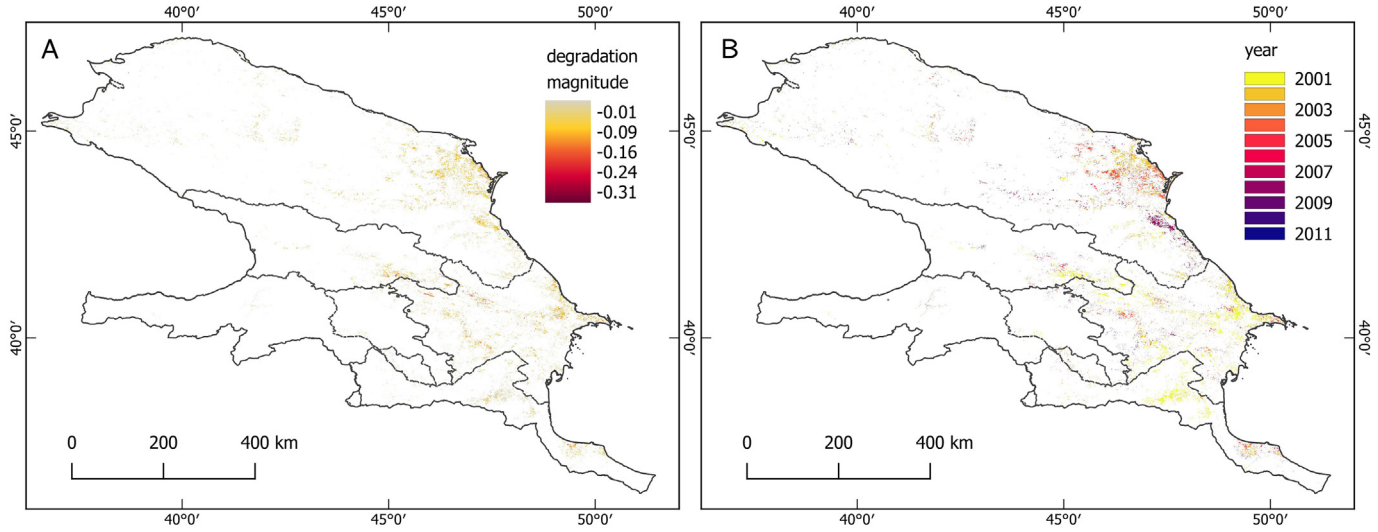

Fig. 9. Magnitude (A) and year of onset (B) of the decadal (≥10 years) degradation episodes. We defined magnitude as the change in green vegetation Cumulative Endmember Fraction between the first and the last year of each trend segment. (For interpretation of the references to colour in this figure legend, the reader is referred to the web version of this article.)

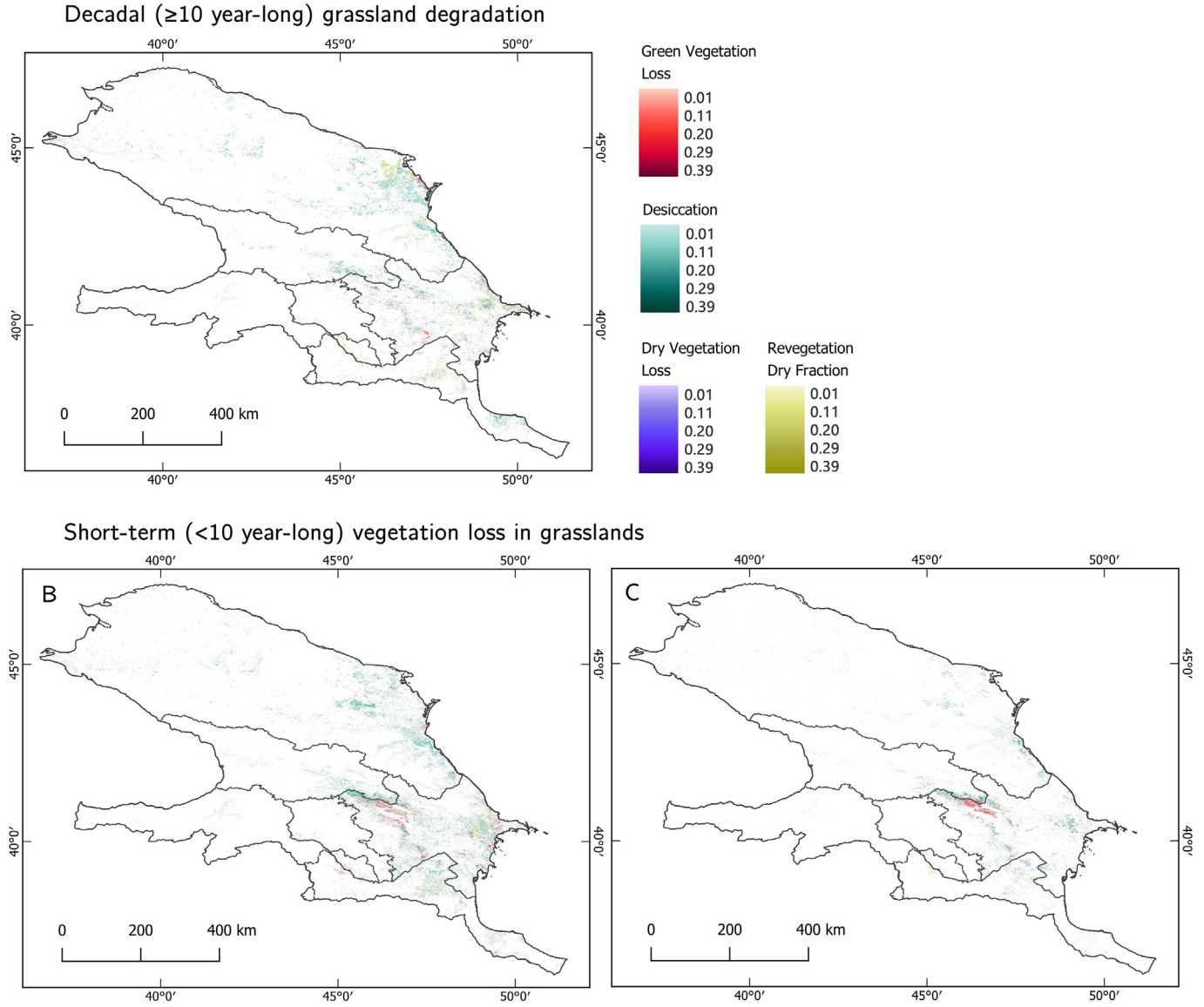

Fig. 10. A: Dominant change pathways for decadal (≥ 10 year-long) grassland degradation between 2001 and 2018. B and C: Dominant change pathways for short-term (< 10 year-long) vegetation loss episodes in grasslands between 2001 and 2018 for the first and second vegetation loss episode, respectively. Values represent a pathway-specific per-pixel magnitude, i.e., change in green vegetation Cumulative Endmember Fraction between the first and the last year of each trend segment. Colour ramps are the same for short-term and decadal episodes. For short-term vegetation loss episodes 3 and 4 see Fig. S3. (For interpretation of the references to colour in this figure legend, the reader is referred to the web version of this article.)

4. Discussion

4.1. Cumulative endmember fractions

We developed a new approach to monitor both short-term vegetation loss and decadal degradation in grasslands that integrates SMA of dense satellite data time series and temporal segmentation for change detection. Our method is physically based and suitable for all grassland ecosystems. A major strength of our approach is that it identifies the spatio-temporal pattern of changes and detects the onset timing and magnitude of vegetation loss episodes of various length. Furthermore, changes among the annual cumulative endmember fractions determine symptomatic pathways of vegetation loss, which helps identifying underlying vegetation loss mechanisms.

Our method can be implemented for any time series of remotely sensed data as long as at least monthly observations are available. The relative temporal change detection does not require 'normal' conditions to train an algorithm, making the approach suited for monitoring of new or continuing degradation processes alike. Moreover, precise identification of endmembers spectra is less critical for change trajectories compared with single-date SMA, which means that Cumulative Endmember Fractions could be applied widely and are suitable for different grassland ecosystems. Importantly, the annual Cumulative Endmember Fractions normalize topographic effects and inter-annual variability of phenology, and allow for direct comparison among years even in complex and diverse regions (for reference see the variation in phenology patterns across the Caucasus Ecoregion approximated by the date of green peak in Fig. S5). This is advantageous compared to analyzing single observations per year (Hostert et al., 2003), or annual composites (Sonnenschein et al., 2011; Suess et al., 2018). Finally, Cumulative Endmember Fractions will capture shifts in phenology patterns, such as change in growing season length, which, among others, can be indicative of long-term trends caused by climate change (Ivits et al., 2012).

The overall accuracy of our approach reflects uncertainty and errors originating from both the SMA and the temporal segmentation. The

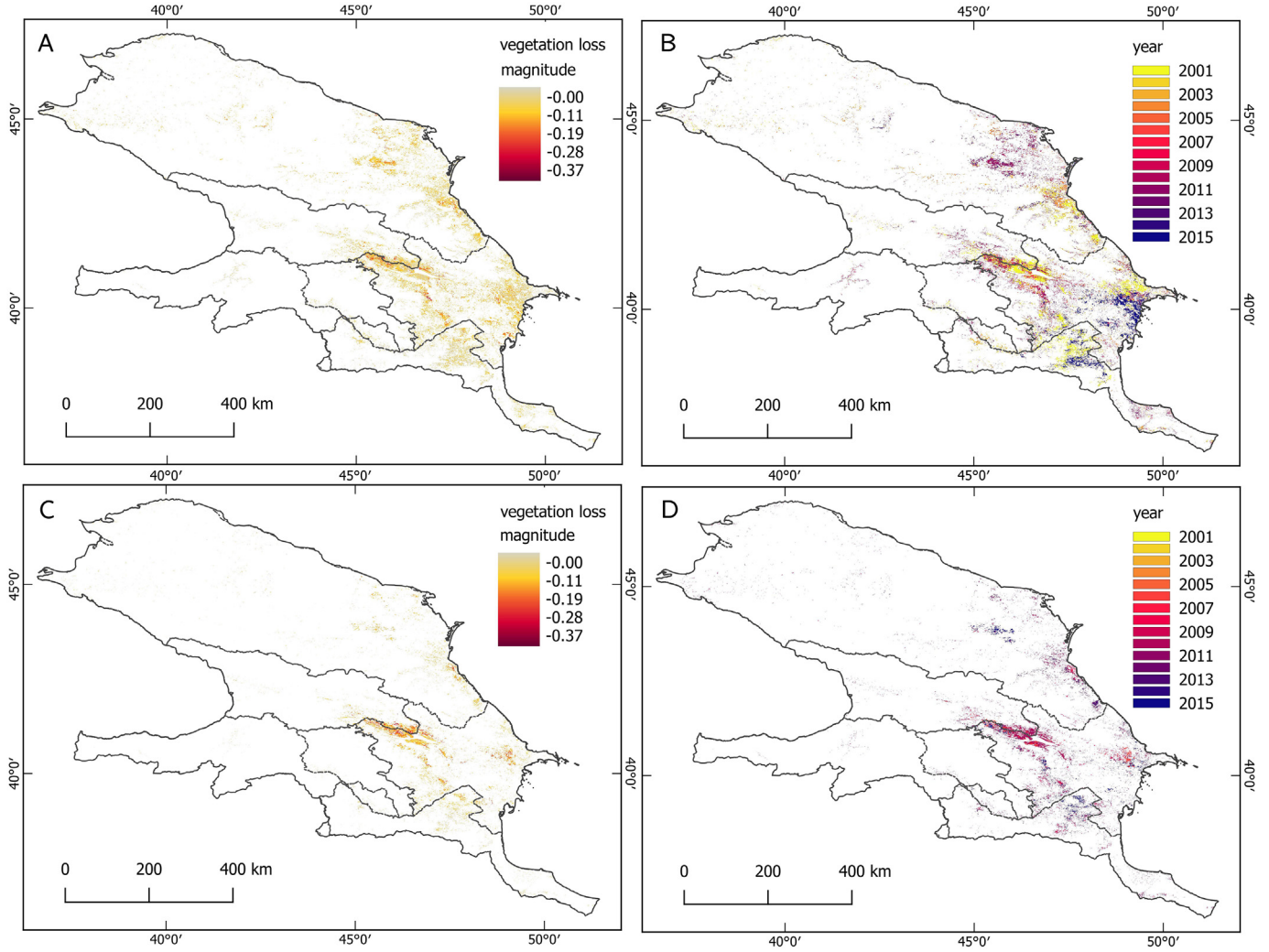

Fig. 11. Magnitude (A, C) and year of onset (B, D) of short-term (< 10 year-long) vegetation loss episodes. Episodes 1 and 2 are presented in the top and bottom row, respectively. Episodes 3 and 4 in Fig. S4. We defined magnitude as the change in green vegetation Cumulative Endmember Fraction between the first and the last year of each trend segment. (For interpretation of the references to colour in this figure legend, the reader is referred to the web version of this article.)

SMA results rely on regional and temporal representativeness of the endmembers. The method can potentially be less accurate for areas undergoing extensive change in vegetation composition, or soils properties, which could lead to substantial alternation in regional green vegetation, non-photosynthetic vegetation or soil spectra during the analyzed time period. However, our findings suggest that our method is robust to changes in endmember sets (Supplement S2). We observed very limited inter- and intra-annual variability in soil and green vegetation endmembers, and all candidate image endmembers identified across different years and seasons had very similar spectra. Moreover,

Table 1
Area of short-term vegetation loss and decadal degradation within the most abundant Natural Vegetation zones (stratification after Bohn et al., 2004).

	Vegetation description	Area [km^2]	Grassland [%]	Vegetation loss [km^2]		Vegetation loss [%]	
				Decadal	Short-term	Decadal	Short-term
B.2	Alpine vegetation	14,300	77.3	< 25	< 25	0.0	0.0
C.3	Subalpine vegetation	38,050	72.8	125	425	0.5	1.5
D.4	Montane and altimontane	10,200	22.8	< 25	< 25	0.0	0.0
F.6	Oriental beech forest	33,200	32.7	225	825	2.1	7.6
F.7	Caucasian mixed oak forests	68,925	28.1	1375	5400	7.1	27.8
H	Hygrophilous mixed forests	7825	22.7	75	400	4.2	22.5
L.1	Subcontinental meadow steppe	25,125	15.1	175	375	4.6	9.9
M.1	True steppe	149,550	24.4	2650	10,525	7.3	28.9
M.2	Desert steppe	34,825	74.7	2300	4625	8.8	17.8
O.2	Sub-shrub deserts	37,350	66.8	2425	11,900	9.7	47.7
P.2	Halophytic vegetation	8000	74.1	1150	2625	19.4	44.3
R	Reed vegetation	21,950	11.0	525	625	21.6	25.8
U.3	Wet lowland forests	12,425	22.7	400	1425	14.2	50.4

For full names of vegetation formations, see Table S2, and for their distribution Fig. S1. Area reported with precision of 25 km^2.

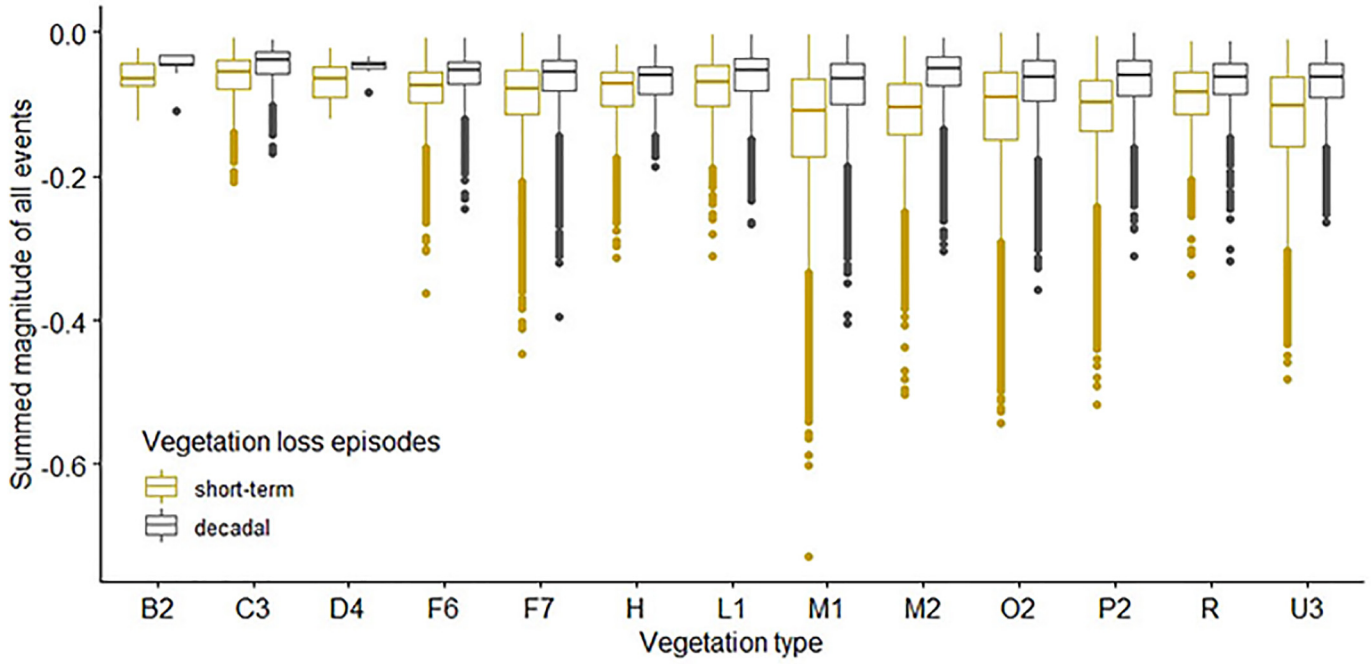

Fig. 12. Box-charts of the per-pixel summed green vegetation loss magnitude of each short-term vegetation loss and decadal degradation episode in each natural vegetation classes. For short class names, see Table 1, or Table S2 for full names, and for a map of natural vegetation view Fig. S1. (For interpretation of the references to colour in this figure legend, the reader is referred to the web version of this article.)

Table 2
Share of dominant vegetation loss change pathways within short-term vegetation loss and decadal degradation areas in the most abundant natural vegetation formations.

Vegetation type	Decadal degradation [% of degraded area]				Short-term vegetation loss [% of degraded area]			
	GVL	D	DVL	DR	GVL	D	DVL	DR
B.2	0.0	0.0[a]	0.0	0.0[a]	0.0[a]	0.0[a]	0.0[a]	0.0[a]
C.3	0.0[a]	75.0	0.0[a]	25.0	11.8	76.5	0.0[a]	11.8
D.4	0.0	0.0[a]	0.0	0.0	0.0[a]	0.0[a]	0.0[a]	0.0[a]
F.6	10.0	80.0	0.0[a]	10.0	6.1	90.9	0.0[a]	3.0
F.7	11.1	81.5	0.0[a]	7.4	9.8	86.5	0.5	3.3
H	0.0[a]	100.0	0.0[a]	0.0[a]	5.9	94.1	0.0[a]	0.0[a]
L.1	14.3	71.4	0.0[a]	14.3	6.7	80.0	0.0[a]	13.3
M.1	10.5	78.1	1.0	10.5	12.1	78.6	0.7	8.6
M.2	12.0	71.7	1.1	15.2	8.6	88.6	0.5	2.2
O.2	30.9	45.4	8.2	15.5	30.0	55.1	4.4	10.5
P.2	23.9	54.3	2.2	19.6	38.5	49.0	2.9	9.6
R	4.8	85.7	0.0[a]	9.5	12.5	83.3	0.0[a]	4.2
U.3	12.5	81.3	0.0[a]	6.3	17.2	72.4	1.7	8.6

For full names of vegetation formations, see Table S2. Abbreviations: GVL – green vegetation loss; D – desiccation; DVL – dry vegetation loss; DR – re-vegetation dry fraction.
[a] Area $< 25\,km^2$.

the SMA RMSE of monthly composites was also, in general, low (Fig. S6). This lends support to the monthly SMA results, and the derived Cumulative Endmember Fractions. However, we caution that spectral stability observed in the Caucasus may not be representative for other grassland areas.

The second source of uncertainty in our method originates from LandTrendr temporal segmentation. The RMSE of the LandTrendr fit showed overall good performance (Fig. S7). To avoid false vegetation loss episodes of small magnitude (Kennedy et al., 2010), we implemented a minimum magnitude threshold of 10% of the per-pixel maximum green vegetation Cumulative Endmember Fraction. This threshold ensured high sensitivity of vegetation-loss detection, but was clearly higher than the MODIS signal to noise ratio (Xiong et al., 2008). The pixel-specific definition of degradation combined with relative change detection in the LandTrendr resulted in non-homogeneous sensitivity of our method to vegetation loss. We overcame this shortcoming by narrowing our analyzes to vegetation loss episodes lasting at least three years, which limited potential false positive responses, and better reflected physical processes we were interested in.

To make our results more interpretable, we combined shade and non-photosynthetic vegetation Cumulative Endmember Fractions into one cumulative fraction. Due to the expected cyclic variability of the shade fraction in grassland ecosystems (arising from phenology-related micro-shading and regional-level change in illumination conditions), this step should not affect accuracy of our method in the Caucasus because shrub coverage is low. However, when applying the method to grassland ecosystems characterized by considerable shrub coverage, or shrub encroachment, we recommend analyzing all four endmembers separately.

A lack of ground truth data precluded an independent validation of our method in the Caucasus. Instead we compared green vegetation Cumulative Endmember Fraction with annual NDVI (Fig. S9) to better understand the differences and similarities between a widely-used vegetation index and our approach. As expected, we observed strong similarity between both time series. However, endmember-based fraction analyses create a linear relationship to vegetation cover, and show higher sensitivity to vegetation fractions and the changes therein when vegetation cover is sparse (Camacho-De Coca et al., 2004). Ultimately, the low RMSE of our spectral unmixing approach, as well as the proven applicability of LandTrendr for time series analyses in grasslands (Dara et al., 2020) support the reliability of our results.

4.2. Short-term vegetation loss and decadal degradation in grasslands in the Caucasus

We implemented our short-term vegetation loss and decadal degradation monitoring approach for the Caucasus Ecoregion, analyzed MODIS 8-day reflectance data for 2001 through 2018 and showed that on average, 9.3% of grasslands in the region were affected by

vegetation loss each year. Vegetation loss was the most widespread in the eastern Caucasus, i.e., in Azerbaijan, Iran, and Dagestan. Those are the driest parts of the Caucasus (Volodicheva, 2002), with annual precipitation often below 400 mm and the potential natural vegetation represented by halophytic, desert- and semi-desert natural vegetation formations. Many of those vegetation loss areas are winter pastures that have been overgrazed (NACRES, 2013; Neudert et al., 2013; Shatberashvili et al., 2015). Surprisingly, our results showed that reed and alluvial vegetation formations also experienced considerable degradation. This may be due to reduced water availability, salinization or increasing land-use pressure (UNEP, 2011).

We detected very limited short-term vegetation loss and degradation in grassland in alpine, subalpine, and montane areas (mostly < 25 km^2 per vegetation class). This may be due to higher natural resilience of those ecosystems or more favorable climate. However, mountain pasture in the region are frequently overgrazed (Belonovskaya, 1995; De Leeuw et al., 2019; Shatberashvili et al., 2015). We speculate that three factors could have influenced our results. First, the resolution and geometric accuracy of the MOD09A1 product may not be sufficient to assess mountain grasslands in the region. Second, our minimum length of vegetation loss episode (3 years) may have been too long to capture localized overgrazing, which may be abrupt (i.e., a single grazing season) and followed by gradual revegetation. Third, some grasslands at high elevations were excluded from the Cumulative Endmember Fractions time series because of snow cover in winter. For mountain meadows, it may be advantageous to calculate Cumulative Endmember Fractions during the growing season only, given that grazing or other forms of land use occur only during the snow-free period.

We identified several hotspots of vegetation loss in grasslands in the Caucasus. The greatest, and at the same time the most dynamic changes were detected along the borderline between western Azerbaijan and eastern Georgia, namely in the surroundings of the Mingachevir Reservoir, on the Iori Plateau, and in Jeyranchol. In these areas, we detected decadal degradation, as well as up to four consecutive short-term vegetation loss episodes, some of which had high magnitude. Green vegetation loss and desiccation were two dominant change pathways in the region, which is in line with the local dry climate (Volodicheva, 2002), and grazing pressure (NACRES, 2013; Shatberashvili et al., 2015; UNFCCC, 2010). Short-term vegetation loss onsets observed in 2011 in the surroundings of the Mingachevir Reservoir corresponded with regional drought conditions, captured in the TerraClim Palmer Drought Severity Index dataset (Abatzoglou et al., 2018) (Fig. S8). We observed a similar pattern in 2016 in Dagestan – another region known for its winter pastures. Since our method provides symptomatic changes only, which, although, to some extent can provide an explanation on the mechanisms related to the observed changes, the exact link between drivers and changes is not possible in the current implementation of the method. Desiccation was the dominant change pathway in the Caucasus Ecoregion, which corresponds well with the increasing dryness of the local climate (Elizbarashvili et al., 2017; Shatberashvili et al., 2015; Zoï Environment Network, 2011), and regional precipitation variability (Fig. S8). Furthermore, brittle environment aids accumulation of vegetation litter that may delay biological decay processes. At the same time, intensive and extensive grazing is expected to reduce green and dry vegetation cover. High frequency of localized reoccurring short-term vegetation loss episodes indicates elevated vegetation stress conditions that, if persistent, may lead to long-term degradation, or even desertification. Consequently, monitoring short-term vegetation loss is of high importance in the region.

Overall, short-term vegetation loss episodes were more frequent and had higher magnitudes than decadal degradation, which is typical for dry regions across the Northern Hemisphere (de Jong et al., 2012). Short-term vegetation loss was spatially and temporally clustered and the obtained spatial pattern better corresponded with known locations of winter pastures than those for decadal degradation. This implies short-term vegetation loss could be more associated with land use and management, in particular, intensive and extensive grazing under arid conditions.

5. Conclusions

Degradation affects one-third of the global land area (FAO, 2015) and is spreading rapidly. Efficient and accurate mapping of short-term vegetation loss and decadal degradation is crucial to improve the understanding of degradation phenomena, to support sustainable land management, and to meet the Land Degradation Neutrality goals (Cowie et al., 2018; UNCCD, 2017b; Vogt et al., 2011). We developed a new approach to monitor both short-term vegetation loss and decadal degradation in grasslands, and applied it to a 2001–2018 MODIS 8-day reflectance data time series of the Caucasus Ecoregion. Our resulting maps showed widespread vegetation loss in the Caucasus and we found that short-term vegetation loss was more frequent and related to greater green vegetation loss magnitudes than decadal degradation. This highlights the importance of monitoring both long- and short-term vegetation trajectories. Timely identification of short-term vegetation loss, is crucial for achieving Land Degradation Neutrality goals, to optimizing grazing pressure, and it provides the information needed to prevent long-term degradation processes, or desertification.

To the best of our knowledge, our analysis is the first wall-to-wall study of short-term vegetation loss and decadal degradation in grassland in the Caucasus. As such, our results contribute to discussions about land degradation in the region, and can inform local land management activities, supporting, among others, stock allocation. Our approach advances the state-of-the-art in short-term vegetation loss and land degradation mapping, specifically for grasslands under grazing regimes, and thereby provides valuable information for carbon stock analyses, sustainable land management, and biodiversity conservation.

Last but not least, annual Cumulative Endmember Fractions can be calculated for any vegetation type, not just grasslands, and can capture the regeneration of vegetation just as easily as degradation. Its physically-based foundation makes our approach easily adaptable to other ecosystems and change processes, but it was beyond the scope of our study to test this.

Declaration of Competing Interest

None.

Acknowledgements

We gratefully acknowledge support from the Land Cover and Land Use Change (LCLUC) Program of the National Aeronautic Space Administration (NASA), Grants 80NSSC18K0316 and 80NSSC18K0343. We thank H. Yin and E. Razenkova for their support, and A. Rizayeva for sharing her first-hand knowledge about the area. We acknowledge E. Askerov, S. Mamadov, A. Abbasov and N. Kasimova for their help during our visit to Azerbaijan in July 2019, and for valuable discussions on land degradation in the region. Finally, we express our gratitude to two anonymous reviewers whose comments significantly improved the quality of the paper.

Appendix A. Supplementary data

Supplementary data to this article can be found online at https://doi.org/10.1016/j.rse.2020.111969.

References

Abatzoglou, J.T., Dobrowski, S.Z., Parks, S.A., Hegewisch, K.C., 2018. TerraClimate, a high-resolution global dataset of monthly climate and climatic water balance from

1958-2015. Sci. Data 5, 1–12. https://doi.org/10.1038/sdata.2017.191.
Adams, J.B., Smith, M.O., 1986. Spectral mixture modeling ' a new analysis of rock and soil types at the Viking Lander 1 site. J. Geogr. Res. 91, 8098–8112. https://doi.org/10.1029/JB091iB08p08098.
Andrade, B.O., Koch, C., Boldrini, I.I., Vélez-Martin, E., Hasenack, H., Hermann, J.M., Kollmann, J., Pillar, V.D., Overbeck, G.E., 2015. Grassland degradation and restoration: a conceptual framework of stages and thresholds illustrated by southern Brazilian grasslands. Nat. e Conserv. 13, 95–104. https://doi.org/10.1016/j.ncon.2015.08.002.
Aronson, J., Alexander, S., 2013. Ecosystem restoration is now a global priority: time to roll up our sleeves. Restor. Ecol. 21, 293–296. https://doi.org/10.1111/rec.12011.
Bai, Z.G., Dent, D.L., Olsson, L., Schaepman, M.E., 2008. Proxy global assessment of land degradation. Soil Use Manag. 24, 223–234. https://doi.org/10.1111/j.1475-2743.2008.00169.x.
Balkovič, J., Skalský, R., Folberth, C., Khabarov, N., Schmid, E., Madaras, M., Obersteiner, M., van der Velde, M., 2018. Impacts and uncertainties of +2°C of climate change and soil degradation on European crop calorie supply. Earth's Futur. 6, 373–395. https://doi.org/10.1002/2017EF000629.
Barbut, M., Alexander, S., 2015. Land Degradation as a Security Threat Amplifier: The New Global Frontline, Land Restoration: Reclaiming Landscapes for a Sustainable Future. Elsevier Inchttps://doi.org/10.1016/B978-0-12-801231-4.00001-X.
Belonovskaya, E.A., 1995. The human-induced transformation of the ecosystems of the Caucasus Mountains. In: Breymeyer, A. (Ed.), Euro-MAB IV. Conference Mountain Zonality Facing Global Change. Institute Geografii i prestrezennego Zagospodarowania, Polska Academia nauk, Warszawa, Warsaw, pp. 42–57.
Belonovskaya, E., Gracheva, R., Shorkunov, I., Vinogradova, V., 2016. Grasslands of intermontane basins of Central Caucasus: land use legacies and present-day state. Hacquetia 15, 37–47. https://doi.org/10.1515/hacq-2016-0016.
Bleyhl, B., Baumann, M., Griffiths, P., Heidelberg, A., Manvelyan, K., Radeloff, V.C., Zazanashvili, N., Kuemmerle, T., 2017. Assessing landscape connectivity for large mammals in the Caucasus using Landsat 8 seasonal image composites. Remote Sens. Environ. 193, 193–203. https://doi.org/10.1016/j.rse.2017.03.001.
Bohn, U., Gollub, G., Hettwer, C., Neuhäuslová, Z., Raus, T., Schlüter, H., Gis, H.W., 2004. Karte der natürlichen Vegetation Europas / Map of the Natural Vegetation of Europe Maßstab / Scale 1 : 2 500 000. Bundesamt für Naturschutz / Federal Agency for Nature Conservation, Bonn, Germany.
Bohn, U., Zazanashvili, N., Nakhutsrishvili, G., 2007. The map of the natural vegetation of Europe and its application in the Caucasus ecoregion. Bull. Georg. Natl. Acad. Sci. 175, 112–121.
Buchner, J., Yin, H., Frantz, D., Kuemmerle, T., Bleyhl, B., Bakuradze, T., Elizbarashvili, N., Komarova, A., Lewińska, K.E., Rizayeva, A., Sayadyan, H., Tan, B., Tepanosyan, G., Zazanashvili, N., Radeloff, V.C., 2020. Land-cover change in the Caucasus Mountains since 1987 based on topographic correction of multi-temporal Landsat composites. Remote Sens. Environ (in review).
Bullock, E.L., Woodcock, C.E., Olofsson, P., 2018. Monitoring tropical forest degradation using spectral unmixing and Landsat time series analysis. Remote Sens. Environ. 110968. https://doi.org/10.1016/j.rse.2018.11.011.
Bullock, E.L., Woodcock, C.E., Holden, C.E., 2019. Improved change monitoring using an ensemble of time series algorithms. Remote Sens. Environ. https://doi.org/10.1016/j.rse.2019.04.018.
Camacho-De Coca, F., García-Haro, F.J., Gilabert, M.A., Meliá, J., 2004. Vegetation cover seasonal changes assessment from TM imagery in a semi-arid landscape. Int. J. Remote Sens. 25, 3451–3476. https://doi.org/10.1080/01431160310001618761.
Caucasus Environment Outlook, 2002. Industrial Wastes. Tbilisi.
Cherlet, M., Hutchinson, C., Reynolds, J., Hill, J., Sommer, S., von Maltitz, G. (Eds.), 2018. World Atlas of Desertification. Publication Office of the European Union, Luxembourg. https://doi.org/10.2760/9205.
Cowie, A.L., Penman, T.D., Gorissen, L., Winslow, M.D., Lehmann, J., Tyrrell, T.D., Twomlow, S., Wilkes, A., Lal, R., Jones, J.W., Paulsch, A., Kellner, K., Akhtar-Schuster, M., 2011. Towards sustainable land management in the drylands: scientific connections in monitoring and assessing dryland degradation, climate change and biodiversity. L. Degrad. Dev. 22, 248–260. https://doi.org/10.1002/ldr.1086.
Cowie, A.L., Orr, B.J., Castillo Sanchez, V.M., Chasek, P., Crossman, N.D., Erlewein, A., Louwagie, G., Maron, M., Metternicht, G.I., Minelli, S., Tengberg, A.E., Walter, S., Welton, S., 2018. Land in balance: the scientific conceptual framework for land degradation neutrality. Environ. Sci. Pol. 79, 25–35. https://doi.org/10.1016/j.envsci.2017.10.011.
Dara, A., Baumann, M., Freitag, M., Hölzel, N., Hostert, P., Kamp, J., Müller, D., Prishchepov, A.V., Kuemmerle, T., 2020. Annual Landsat time series reveal post-soviet changes in grazing pressure. Remote Sens. Environ. 239, 111667. https://doi.org/10.1016/j.rse.2020.111667.
Daughtry, C.S.T., Hunt, E.R., 2008. Mitigating the effects of soil and residue water contents on remotely sensed estimates of crop residue cover. Remote Sens. Environ. 112, 1647–1657. https://doi.org/10.1016/j.rse.2007.08.006.
de Jong, R., De Bruin, S., De Wit, A., Schaepman, M.E., Dent, D.L., 2011. Analysis of monotonic greening and browning trends from global NDVI time-series. Remote Sens. Environ. 115, 692–702. https://doi.org/10.1016/j.rse.2010.10.011.
de Jong, R., Verbesselt, J., Schaepman, M.E., de Bruin, S., 2012. Trend changes in global greening and browning: contribution of short-term trends to longer-term change. Glob. Chang. Biol. 18, 642–655. https://doi.org/10.1111/j.1365-2486.2011.02578.x.
De Leeuw, J., Rizayeva, A., Namazov, E., Bayramov, E., Marshall, M.T., Etzold, J., Neudert, R., 2019. Application of the MODIS MOD 17 net primary production product in grassland carrying capacity assessment. Int. J. Appl. Earth Obs. Geoinf. 78, 66–76. https://doi.org/10.1016/j.jag.2018.09.014.
Dlamini, P., Chivenge, P., Manson, A., Chaplot, V., 2014. Land degradation impact on soil organic carbon and nitrogen stocks of sub-tropical humid grasslands in South Africa. Geoderma 235–236, 372–381. https://doi.org/10.1016/j.geoderma.2014.07.016.
Dubovyk, O., 2017. The role of remote sensing in land degradation assessments: opportunities and challenges. Eur. J. Remote Sens. 50, 601–613. https://doi.org/10.1080/22797254.2017.1378926.
Dubovyk, O., Menz, G., Conrad, C., Kan, E., Machwitz, M., Khamzina, A., 2013. Spatio-temporal analyses of cropland degradation in the irrigated lowlands of Uzbekistan using remote-sensing and logistic regression modeling. Environ. Monit. Assess. 185, 4775–4790. https://doi.org/10.1007/s10661-012-2904-6.
Eckert, S., Hüsler, F., Liniger, H., Hodel, E., 2015. Trend analysis of MODIS NDVI time series for detecting land degradation and regeneration in Mongolia. J. Arid Environ. 113, 16–28. https://doi.org/10.1016/j.jaridenv.2014.09.001.
Elizbarashvili, M., Elizbarashvili, E., Tatishvili, M., Elizbarashvili, S., Meskhia, R., Kutaladze, N., King, L., Keggenhoff, I., Khardziani, T., 2017. Georgian climate change under global warming conditions. Ann. Agrar. Sci. 15, 17–25. https://doi.org/10.1016/j.aasci.2017.02.001.
Elmore, A.J., Mustard, J.F., Manning, S.J., Lobell, D.B., 2000. Quantifying vegetation change in semiarid environments: precision and accuracy of spectral mixture analysis and the normalized difference vegetation index. Remote Sens. Environ. 102, 87–102. https://doi.org/10.1016/S0034-4257(00)00100-0.
FAO, 2011. The State of the World's Land and Water Resources for Food and Agriculture. The Food and Agriculture Organization of the United Nations and Earthscan. (doi:978-1-84971-326-9).
FAO, 2015. Status of the World's Soil Resources Main Report. (Rome).
Fensholt, R., Proud, S.R., 2012. Remote sensing of environment evaluation of earth observation based global long term vegetation trends — comparing GIMMS and MODIS global NDVI time series. Remote Sens. Environ. 119, 131–147. https://doi.org/10.1016/j.rse.2011.12.015.
Fensholt, R., Rasmussen, K., Kaspersen, P., Huber, S., Horion, S., Swinnen, E., 2013. Assessing land degradation / recovery in the African Sahel from long-term earth observation based primary. Remote Sens. 5, 664–686. https://doi.org/10.3390/rs5020664.
Gao, Q., Li, Y., Wan, Y., Lin, E., Xiong, W., Jiangcun, W., Wang, B., Li, W., 2006. Grassland degradation in northern Tibet based on remote sensing data. J. Geogr. Sci. 16, 165–173. https://doi.org/10.1007/s11442-006-0204-1.
Gao, F., Masek, J., Schwaller, M., Hall, F., 2006. On the blending of the MODIS and Landsat ETM + surface reflectance:predicting daily Landsat Surface Reflectanc. IEEE Trans. Geosci. Remote Sens. 44, 2207–2218. https://doi.org/10.1109/TGRS.2006.872081.
Gao, Q., Wan, Y., Xu, H., Li, Y., Jiangcun, W., Borjigidai, A., 2010. Alpine grassland degradation index and its response to recent climate variability in northern Tibet, China. Quat. Int. 226, 143–150. https://doi.org/10.1016/j.quaint.2009.10.035.
Gibbs, H.K., Salmon, J.M., 2015. Mapping the world's degraded lands. Appl. Geogr. 57, 12–21. https://doi.org/10.1016/j.apgeog.2014.11.024.
Gisladottir, G., Stocking, M., 2005. Land degradation control and its global environmental benefits. L. Degrad. Dev. 16, 99–112. https://doi.org/10.1002/ldr.687.
Gorelick, N., Hancher, M., Dixon, M., Ilyushchenko, S., Thau, D., Moore, R., 2017. Google earth engine: planetary-scale geospatial analysis for everyone. Remote Sens. Environ. 202, 18–27. https://doi.org/10.1016/j.rse.2017.06.031.
Hassan, R., Scholes, R., Ash, N. (Eds.), 2005. Ecosystems and Human Well-being : Current State and Trends, 1st ed. 1 Millennium Ecosystem Assessment. Island Press, Washington, Covelo, London.
Hilker, T., Wulder, M.A., Coops, N.C., Linke, J., McDermid, G., Masek, J.G., Gao, F., White, J.C., 2009. A new data fusion model for high spatial- and temporal-resolution mapping of forest disturbance based on Landsat and MODIS. Remote Sens. Environ. 113, 1613–1627. https://doi.org/10.1016/j.rse.2009.03.007.
Hobi, M.L., Dubinin, M., Graham, C.H., Coops, N.C., Clayton, M.K., Pidgeon, A.M., Radeloff, V.C., 2017. A comparison of dynamic habitat indices derived from different MODIS products as predictors of avian species richness. Remote Sens. Environ. 195, 142–152. https://doi.org/10.1016/j.rse.2017.04.018.
Horion, S., Fensholt, R., Tagesson, T., Ehammer, A., 2014. Using earth observation-based dry season NDVI trends for assessment of changes in tree cover in the Sahel. Int. J. Remote Sens. 35, 2493–2515. https://doi.org/10.1080/01431161.2014.883104.
Hostert, P., Röder, A., Hill, J., Udelhoven, T., Tsiourlis, G., 2003. Retrospective studies of grazing-induced land degradation: a case study in Central Crete, Greece. Int. J. Remote Sens. 24, 4019–4034. https://doi.org/10.1080/0143116031000103844.
Huang, C., Goward, S.N., Masek, J.G., Thomas, N., Zhu, Z., Vogelmann, J.E., 2010. An automated approach for reconstructing recent forest disturbance history using dense Landsat time series stacks. Remote Sens. Environ. 114, 183–198. https://doi.org/10.1016/j.rse.2009.08.017.
Huete, A.R., Jackson, R.D., Post, D.F., 1985. Spectral response of a plant canopy with different soil backgrounds. Remote Sens. Environ. 17, 37–53. https://doi.org/10.1016/0034-4257(85)90111-7.
IPCC, 2019. Special Report on Climate Change and Land, Ipcc.
Ivits, E., Cherlet, M., Tóth, G., Sommer, S., Mehl, W., Vogt, J., Micale, F., 2012. Combining satellite derived phenology with climate data for climate change impact assessment. Glob. Planet. Chang. 88–89, 85–97. https://doi.org/10.1016/j.gloplacha.2012.03.010.
Jamsranjav, C., Reid, R.S., Fernández-Giménez, M.E., Tsevlee, A., Yadamsuren, B., Heiner, M., 2018. Applying a dryland degradation framework for rangelands: the case of Mongolia. Ecol. Appl. 28, 622–642. https://doi.org/10.1002/eap.1684.
Kennedy, R.E., Yang, Z., Cohen, W.B., 2010. Detecting trends in forest disturbance and recovery using yearly Landsat time series: 1. LandTrendr - Temporal segmentation algorithms. Remote Sens. Environ. 114, 2897–2910. https://doi.org/10.3899/jrheum.111106.
Kennedy, R.E., Yang, Z., Gorelick, N., Braaten, J., Cavalcante, L., Cohen, W.B., Healey, S.,

2018. Implementation of the LandTrendr algorithm on Google earth engine. Remote Sens. 10, 1–10. https://doi.org/10.3390/rs10050691.
Kuemmerle, T., Röder, A., Hill, J., 2006. Separating grassland and shrub vegetation by multidate pixel-adaptive spectral mixture analysis. Int. J. Remote Sens. 27, 3251–3271. https://doi.org/10.1080/01431160500488944.
Lachashvili, N.J., Khachidze, M.N., Eradze, N.V., Khetsuriani, L.D., 2017. Annals of Agrarian science steppe of Tbilisi environs (East Georgia, South Caucasus). Ann. Agrar. Sci. 15, 332–338. https://doi.org/10.1016/j.aasci.2017.06.003.
Lyapustin, A., Wang, Y., Xiong, X., Meister, G., Platnick, S., Levy, R., Franz, B., Korkin, S., Hilker, T., Tucker, J., Hall, F., Sellers, P., Wu, A., Angal, A., 2014. Scientific impact of MODIS C5 calibration degradation and C6+ improvements. Atmos. Meas. Tech. 7, 4353–4365. https://doi.org/10.5194/amt-7-4353-2014.
Main-Knorn, M., Cohen, W.B., Kennedy, R.E., Grodzki, W., Pflugmacher, D., Griffiths, P., Hostert, P., 2013. Monitoring coniferous forest biomass change using a Landsat trajectory-based approach. Remote Sens. Environ. 139, 277–290. https://doi.org/10.1016/j.rse.2013.08.010.
Mansour, K., Mutanga, O., Adam, E., Abdel-Rahman, E.M., 2016. Multispectral remote sensing for mapping grassland degradation using the key indicators of grass species and edaphic factors. Geocarto Int. 31, 477–491. https://doi.org/10.1080/10106049.2015.1059898.
Marchese, C., 2015. Biodiversity hotspots: a shortcut for a more complicated concept. Glob. Ecol. Conserv. 3, 297–309. https://doi.org/10.1016/j.gecco.2014.12.008.
Mitchard, E.T.A., 2018. The tropical forest carbon cycle and climate change. Nature 559, 527–534. https://doi.org/10.1038/s41586-018-0300-2.
NACRES, 2013. Assessment of Pastures in Vashlovani National Park. Tibilisi.
Neudert, R., Allahverdiyeva, N.K., 2009. Economic performance of transhumant sheep farming in Azerbaijan and prospects for its future development. South Cauc. Ann. Agrar. Sci. 7, 153–157.
Neudert, R., Etzold, J., Münzner, F., Manthey, M., Busse, S., 2013. The opportunity costs of conserving pasture resources for mobile pastoralists in the greater Caucasus. Landsc. Res. 38, 499–522. https://doi.org/10.1080/01426397.2012.728204.
Reed, B.C., Brown, J., VanderZee, D., Loveland, T., Merchant, J., Ohlen, D.O., 1994. Measuring phenological variability from satellite imagery. J. Veg. Sci. 5, 703–714.
Reed, M.S., Buenemann, M., Atlhopheng, J., Akhtar-Schuster, M., Bachmann, F., Bastin, G., Bigas, H., Chanda, R., Dougill, A.J., Essahli, W., Evely, A.C., Fleskens, L., Geeson, N., Glass, J.H., Hessel, R., Holden, J., Ioris, A.A.R., Kruger, B., Liniger, H.P., Mphinyane, W., Nainggolan, D., Perkins, J., Raymond, C.M., Ritsema, C.J., Schwilch, G., Sebego, R., Seely, M., Stringer, L.C., Thomas, R., Twomlow, S., Verzandvoort, S., 2011. Cross-scale monitoring and assessment of land degradation and sustainable land management: a methodological framework for knowledge management. L. Degrad. Dev. 22, 261–271. https://doi.org/10.1002/ldr.1087.
Schultz, M., Clevers, J.G.P.W., Carter, S., Verbesselt, J., Avitabile, V., Quang, H.V., Herold, M., 2016. Performance of vegetation indices from Landsat time series in deforestation monitoring. Int. J. Appl. Earth Obs. Geoinf. 52, 318–327. https://doi.org/10.1016/j.jag.2016.06.020.
Shatberashvili, N., Rucevska, I., Jørstad, H., Artsivadze, K., Mehdiyev, B., Aliyev, M., Fayvush, G., Dzneladze, M., Jurek, M., Kirkfeldt, T., Semernya, L., 2015. Outlook on Climate Change Adaptation in the South Caucasus mountains. United Nations Environment Programme, GRID-Arendal and Sustainable Caucasus, Nairobi, Arendal and Tbilisi. https://doi.org/10.13140/RG.2.1.4311.1287.
Smith, M.O., Ustin, S.L., Adams, J.B., Gillespie, A.R., 1990. Vegetation in deserts: I. A regional measure of abundance from multispectral images. Remote Sens. Environ. 31, 1–26. https://doi.org/10.1016/0034-4257(90)90074-V.
Smith, W.K., Dannenberg, M.P., Yan, D., Herrmann, S., Barnes, M.L., Barron-Gafford, G.A., Biederman, J.A., Ferrenberg, S., Fox, A.M., Hudson, A.R., Knowles, J.F., MacBean, N., Moore, D.J.P., Nagler, P.L., Reed, S.C., Rutherford, W.A., Scott, R.L., Wang, X., Yang, J., 2019. Remote sensing of dryland ecosystem structure and function: Progress, challenges, and opportunities. Remote Sens. Environ. 233, 111401. https://doi.org/10.1016/j.rse.2019.111401.
Somers, B., Asner, G.P., Tits, L., Coppin, P., 2011. Remote sensing of environment end-member variability in spectral mixture analysis: a review. Remote Sens. Environ. 115, 1603–1616. https://doi.org/10.1016/j.rse.2011.03.003.
Song, X.-P., Hansen, M.C., Stehman, S.V., Potapov, P.V., Tyukavina, A., Vermote, E.F., Townshend, J.R., 2018. Global land change from 1982 to 2016. Nature 560, 639–643. https://doi.org/10.1038/s41586-018-0411-9.
Sonnenschein, R., Kuemmerle, T., Udelhoven, T., Stellmes, M., Hostert, P., 2011. Differences in Landsat-based trend analyses in drylands due to the choice of vegetation estimate. Remote Sens. Environ. 115, 1408–1420. https://doi.org/10.1016/j.rse.2011.01.021.
Suess, S., van der Linden, S., Okujeni, A., Griffiths, P., Leitão, P.J., Schwieder, M., Hostert, P., 2018. Characterizing 32 years of shrub cover dynamics in southern Portugal using annual Landsat composites and machine learning regression modeling. Remote Sens. Environ. 219, 353–364. https://doi.org/10.1016/j.rse.2018.10.004.
Tepanosyan, G.H., Asmaryan, S.G., Muradyan, V.S., Saghatelyan, A.K., 2017. Mapping man-induced soil degradation in Armenia's high mountain pastures through remote sensing methods: a case study. Remote Sens. Appl. Soc. Environ. 8, 105–113. https://doi.org/10.1016/j.rsase.2017.08.006.
Tindall, D., Scarth, P., Schmidt, M., Muir, J., Trevithick, R., Denham, R., Pringle, M., Witte, C., 2012. The Queensland ground cover monitoring program. In: ISPRS Congress (Ed.), International Archives of the Photogrammetry, Remote Sensing and Spatial Information Sciences. ISPRS CongressAt, Melbourne, Australia. Melbourne.
Tishkov, A., Belonovskaya, E., 2012. Mountain natiral biodiversity conservation in Russia. Geogr. Environ. Sustan. 5, 51–67. https://doi.org/10.24057/2071-9388-2012-5-2-51-67.
UN General Assembly, 2010. Resolution adopted by the General Assembly on 21 December 2009 [on the report of the Second Committee (A/64/420/Add.5)].
UNCCD, 2017a. UNCCD - ICCD/COP(13)/L.18 - The Future Strategic Framework of the Convention - Draft Decision Submitted by the Chair of the Committee of the Whole 16078. pp. 1–9.
UNCCD, 2017b. Integration of Sustainable Development Goal 15 and Related Target 15.3 Which States: to Combat Desertification, Restore Degraded Land and Soil, Including Land Affected by Desertification, Drought and Floods, and Strive to Achieve a Land Degradation-neutr. Ordos, China. (doi:GE.19-10284(E)).
UNEP, 2011. Caspian Sea State of the Environment, Encyclopedia of Environment and Society.
UNFCCC, 2010. Second national communication to the United Nations framework convention on climate change. Baku. https://doi.org/10.1017/CBO9781107415324.004.
Meer, F.D., Van Der Jia, X., 2012. Collinearity and orthogonality of endmembers in linear spectral unmixing. Int. J. Appl. Earth Obs. Geoinf. 18, 491–503. https://doi.org/10.1016/j.jag.2011.10.004.
Verbesselt, J., Hyndman, R., Newnham, G., Culvenor, D., 2010a. Detecting trend and seasonal changes in satellite image time series. Remote Sens. Environ. 114, 106–115. https://doi.org/10.1016/j.rse.2009.08.014.
Verbesselt, J., Hyndman, R., Zeileis, A., Culvenor, D., 2010b. Phenological change detection while accounting for abrupt and gradual trends in satellite image time series. Remote Sens. Environ. 114, 2970–2980. https://doi.org/10.1016/j.rse.2010.08.003.
Verbesselt, J., Zeileis, A., Herold, M., 2012. Near real-time disturbance detection using satellite image time series. Remote Sens. Environ. 123, 98–108. https://doi.org/10.1016/j.rse.2012.02.022.
Vermote, E.F., El Saleous, N.Z., Justice, C.O., 2002. Atmospheric correction of MODIS data in the visible to middle infrared: first results. Remote Sens. Environ. 83, 97–111. https://doi.org/10.1016/S0034-4257(02)00089-5.
Vogt, J.V., Safriel, U., Von Maltitz, G., Sokona, Y., Zougmore, R., Bastin, G., Hill, J., 2011. Monitoring and assessment of land degradation and desertification: towards new conceptual and integrated approaches. L. Degrad. Dev. 22, 150–165. https://doi.org/10.1002/ldr.1075.
Volodicheva, N., 2002. The physical geography of Northern Eurasia. In: Shahgedanova, M. (Ed.), The Physical Geography of Northern Caucasus. Oxford University Press, pp. 350–376.
Wen, L., Dong, S., Li, Y., Wang, X., Li, X., Shi, J., Dong, Q., 2013. The impact of land degradation on the C pools in alpine grasslands of the Qinghai-Tibet plateau. Plant Soil 368, 329–340. https://doi.org/10.1007/s11104-012-1500-4.
Wessels, K.J., van den Bergh, F., Scholes, R.J., 2012. Limits to detectability of land degradation by trend analysis of vegetation index data. Remote Sens. Environ. 125, 10–22. https://doi.org/10.1016/j.rse.2012.06.022.
Xiong, X., Angal, A., Xie, X., 2008. On-orbit noise characterization for modis reflective solar bands. Int. Geosci. Remote Sens. Symp. 4. https://doi.org/10.1109/IGARSS.2008.4779978.
Yengoh, G.T., Dent, D., Olsson, L., Tengberg, A.E., Tucker III, C.J., 2015. Use of the Normalized Diff erence Vegetation Index (NDVI) to Assess Land Degradation at Multiple Scales Current Status, Future Trends, and Practical Considerations. Springer, Cham. https://doi.org/10.1007/978-3-319-24112-8.
Zazanashvili, N.R., Gagnidze, G., Nakhutsrishvili, 2000. Main types of vegetation zonation on the mountains of the Caucasus. Acta Phytogeogr. Suec. 85, 7–16.
Zhang, X., Niu, J., Buyantuev, A., Zhang, Q., Dong, J., Kang, S., Zhang, J., 2016. Understanding grassland degradation and restoration from the perspective of ecosystem services: a case study of the Xilin River basin in Inner Mongolia, China. Sustain. 8, 1–17. https://doi.org/10.3390/su8070594.
Zhou, W., Yang, H., Huang, L., Chen, C., Lin, X., Hu, Z., Li, J., 2017. Grassland degradation remote sensing monitoring and driving factors quantitative assessment in China from 1982 to 2010. Ecol. Indic. 83, 303–313. https://doi.org/10.1016/j.ecolind.2017.08.019.
Zhu, Z., Woodcock, C.E., 2012. Object-based cloud and cloud shadow detection in Landsat imagery. Remote Sens. Environ. 118, 83–94. https://doi.org/10.1016/j.rse.2011.10.028.
Zhu, X., Chen, J., Gao, F., Chen, X., Masek, J.G., 2010. An enhanced spatial and temporal adaptive reflectance fusion model for complex heterogeneous regions. Remote Sens. Environ. 114, 2610–2623. https://doi.org/10.1016/j.rse.2010.05.032.
Zoï Environment Network, 2011. Climate Change in the South Caucasus. A Visual Synthesis. Austrian Federal Ministry ofAgriculture, Geneva.